

Carbon Enhanced Metal-Poor Stars.

I. Chemical Compositions of 26 Stars¹

Wako Aoki², Timothy C. Beers³, Norbert Christlieb⁴, John E. Norris⁵, Sean G. Ryan^{6,7}, Stelios Tsangarides⁶

ABSTRACT

The chemical compositions of 26 metal-poor stars that exhibit strong CH and/or C₂ molecular bands are determined based on high-resolution spectroscopy. We define carbon-enhanced stars taking account of the carbon abundance ratio ($[C/Fe]$) and the evolutionary status, which is a slight modification over previous definitions. Twenty two stars in our sample satisfy our modified definition for Carbon-Enhanced Metal-Poor (CEMP) stars. In addition, we measure Na abundances for nine other carbon-enhanced stars for which abundances of other elements have been previously reported. Combining our new sample with the results of previous work, we investigate the abundance and evolutionary status of a total of 64 CEMP stars. The following results are obtained: (1) All but one of the 37 stars with $[Fe/H] \geq -2.6$ exhibit large excesses of barium ($[Ba/Fe] > +0.5$), while the other 27 stars with lower metallicity exhibit a large scatter in their barium abundance ratios ($-1.2 < [Ba/Fe] < +3.3$). (2) A correlation between the carbon and barium abundance ratios ($[C/Fe]$ and $[Ba/Fe]$) is found in Ba-enhanced objects (comprising 54 stars), suggesting that the origin of the observed carbon excess in Ba-enhanced stars is nucleosynthesis in asymptotic giant branch (AGB) stars, where the main *s*-process occurs. The correlation between the barium abundance ratio and that of carbon plus nitrogen ($[(C+N)/Fe]$) is relatively weak, because of the large excesses of nitrogen in some extremely metal-poor stars. (3) The majority of the Ba-enhanced stars have $-1.0 < [C/H] < 0.0$, and a clear cutoff exists at $[C/H] \sim 0$, which we take as the limit of carbon-enrichment by metal-poor AGB stars. Within the above range,

²National Astronomical Observatory, Mitaka, Tokyo, 181-8588, Japan; email: aoki.wako@nao.ac.jp

³Dept. of Physics & Astronomy, CSCE: Center for the Study of Cosmic Evolution, and JINA: Joint Institute for Nuclear Astrophysics, Michigan State University, E. Lansing, MI 48824; beers@pa.msu.edu

⁴Hamburger Sternwarte, University of Hamburg, Gojenbergsweg 112, D-21029 Hamburg, Germany; nchristlieb@hs.uni-hamburg.de

⁵Research School of Astronomy and Astrophysics, The Australian National University, Mount Stromlo Observatory, Cotter Road, Weston, ACT 2611, Australia; email: jen@mso.anu.edu.au

⁶Department of Physics and Astronomy, The Open University, Walton Hall, Milton Keynes, MK7 6AA, UK; email: stsangarides@gmail.com

⁷Present address: Centre for Astrophysics Research, STRI and School of Physics, Astronomy and Mathematics, University of Hertfordshire, College Lane, Hatfield AL10 9AB, United Kingdom; s.g.ryan@herts.ac.uk

the $[C/H]$ of the Ba-enhanced CEMP stars decreases, on average, by up to 0.6 dex from the main-sequence turnoff up the red-giant branch, suggesting some dilution of carbon enhancement during their evolution. The $[C/H]$ values of Ba-normal stars are relatively low, with a wide distribution. (4) The difference in the distributions of evolutionary status between Ba-enhanced and Ba-normal CEMP stars suggested by our previous work is not statistically confirmed by the present, enlarged sample. (5) Excesses of Na are found in stars with extremely large enhancements of C, N and Ba, suggesting efficient production of this element by AGB nucleosynthesis. The implications of these results on the origins of carbon in CEMP stars, in particular for Ba-normal stars, are discussed.

Subject headings: nuclear reactions, nucleosynthesis, abundances — stars: abundances — stars: AGB and post-AGB — stars: carbon — stars: Population II

1. Introduction

Large modern surveys of metal-deficient stars in the Galaxy have revealed that the fraction of carbon-enhanced objects is significant at low metallicity (Beers et al. 1992; Christlieb 2003). The fraction appears to increase with decreasing metallicity (Beers & Christlieb 2005; Lucatello et al. 2006), although the derived fraction depends somewhat on one’s choice of the definition of the carbon-enhancement phenomenon. Many years ago, Keenan (1942) coined the term “CH stars” to refer to “high-velocity” carbon stars that exhibit very strong G-bands due to the CH molecule, and otherwise weak lines of other metals usually used to classify stellar spectra. The small sample of stars he had available at that time had spectra that suggested high luminosities, i.e., membership on the giant branch. The nomenclature was extended to objects of lower luminosity by Bond (1974), who found subgiants with similar elemental compositions. More recently, surveys for carbon stars at high Galactic latitude have also been made (Green et al. 1994; Totten & Irwin 1998; Totten, Irwin, & Whitelock 2000; Christlieb et al. 2001). The Carbon-Enhanced Metal-Poor (CEMP) stars found by recent surveys of metal-poor stars may well be closely related to these objects.

An important question concerning the nature of CEMP stars is that of the astrophysical origin of the carbon excess that is observed in these objects. One established scenario is carbon production by nucleosynthesis in an asymptotic giant branch (AGB) star. Since most CEMP stars that are observed in the present Galaxy are too old to be intrinsic AGB stars², it is usually assumed that

¹Based on data collected at the Subaru Telescope, which is operated by the National Astronomical Observatory of Japan.

²There exists one recently-discovered exception, CS 30322–023, which Masseron et al. (2006) argue is likely to be an extremely metal-poor AGB star that is presently undergoing thermal pulses. This star also appears in our present sample.

the AGB star responsible for carbon production was once the primary of a binary system, and the elements produced during its lifetime and dredged to its outer atmosphere were transferred to its companion prior to the primary evolving to become a faint white dwarf. Observational support for this scenario is found from the observed excess of *s*-process elements, as well as carbon, in classical CH stars (e.g. Wallerstein & Greenstein 1963; Vanture 1992) and some CEMP stars (e.g., Norris et al. 1997a). Other evidence comes from the binarity of the objects found in some CH and CEMP stars identified from radial-velocity monitoring (McClure 1984; McClure & Woodsworth 1990; Preston & Sneden 2001). The fraction of binary stars among CEMP stars has been recently studied by Lucatello et al. (2005), who concluded that all CEMP stars with *s*-process element overabundances (which Beers & Christlieb 2005 refer to as CEMP-*s* stars) could statistically belong to binary systems, given the limited observational constraints on the radial-velocity variations observed to date.³

However, in some CEMP stars, no excess of neutron-capture elements is found (e.g., Norris et al. 1997b; Aoki et al. 2002b); these stars are referred to as CEMP-no stars (Beers & Christlieb 2005). At least one CEMP star (CS 22892-052; Sneden et al. 1996) has been reported with an excess of neutron-capture elements associated with the *r*-process. Lucatello et al. (in preparation) has identified a few other such stars, hence the class CEMP-*r* is no longer based on a single object. There are a growing number of CEMP stars with apparent contributions from *both* the *r*-process and the *s*-process, the CEMP-*r/s* stars (see Beers & Christlieb 2005 for further discussion of these classes). The existence of such a wide variety of elemental abundance patterns associated with CEMP stars strongly suggests that other mechanisms may be responsible for their nucleosynthetic history beyond those involving AGB stars. Ryan et al. (2005) compiled the elemental and isotopic abundances of 19 CEMP stars measured by previous work where the $^{13}\text{C}/^{12}\text{C}$ ratio was studied, and considered possible differences between Ba-enhanced CEMP stars (CEMP-*s*) and Ba-normal ones (CEMP-no). This discussion was necessarily somewhat limited because of the small sample size.

Our long-running investigation of these interesting objects has led us to undertake a high-resolution spectroscopic study for an expanded sample of candidate CEMP stars. We have thus far obtained spectra for 26 stars with the Subaru Telescope High Dispersion Spectrograph (Noguchi et al. 2002); we report on their chemical compositions in this paper. We also analyze redder spectra, in order to measure their Na abundances, for another nine stars for which abundances of other elements have been reported by previous work. Based on the results of our present abundance study and on previous work, we discuss the distribution of the carbon-enhancement, the fraction of Ba-enhanced stars, and the metallicity distribution among CEMP stars. The evolutionary status of our sample is taken into consideration in our discussion. The sample selection, observations, and

³Contributions of the *s*- and *r*- processes are estimated from the abundance ratios of neutron-capture elements such as [Ba/Fe], [Eu/Fe], and [Ba/Eu]. For instance, the term ‘*s*-process element-enhanced stars’ indicates objects that have high [Ba/Fe](> +0.5) and high [Ba/Eu] ($\sim +1$).

data-reduction procedures are reported in §2. Details of the abundance analyses are presented in §3. Our modified definition of carbon-enhanced objects is given in §4. We discuss the abundance distribution of barium and the differences between the Ba-enhanced and Ba-normal stars in §5. In §6 we present our conclusions.

2. Observations and Measurements

2.1. Sample Selection and Photometry

Stars in our main program were selected on the basis of medium-resolution spectroscopic follow-up of metal-poor candidates from the HK survey (Beers et al. 1992; Beers 1999) and the Hamburg/ESO survey (HES; Christlieb 2003) that exhibited apparently strong CH G bands and metallicities of $[\text{Fe}/\text{H}] < -2.0$.⁴ The majority of the HES stars considered in the present paper were drawn from the list of carbon-enhanced stars of Christlieb et al. (2001), which sought to identify stars on the basis of their carbon enhancement, rather than low metallicity. The list of objects is provided in Table 1, where coordinates and details of the observations are given. We note that HE 0039–2635 is identical to CS 29497–034, which was studied in detail by Barbuy et al. (1997), Hill et al. (2000), and Barbuy et al. (2005). This star was re-identified as a candidate CEMP star by the HES.

Effective temperatures for the stars in our sample are estimated from photometric data using the color-temperature relation provided by Alonso, Arribas, & Martínez-Roger (1996) and Alonso, Arribas, & Martínez-Roger (1999) (see §3.1). Optical *BVR*I photometry (Johnson-Kron-Cousins) for these stars are reported by Beers et al. (2006). The results are listed in Table 2. Errors in the photometric measurements are typically on the order of 0.01–0.02 mag. Near infrared *JHK* photometry was collected from the database of the Two Micron All Sky Survey (2MASS) Point Source Catalog (Skrutskie et al. 2006). Table 2 also lists our adopted estimates of interstellar reddening ($E(B - V)$), which are total line-of-sight values derived from the dust map of Schlegel, Finkbeiner, & Davis (1998). The extinction in each band is obtained from the reddening relation provided in their Table 6.

2.2. High-Resolution Spectroscopy

High-resolution spectroscopic observations for the stars in our sample was obtained with Subaru/HDS, with a spectral resolving power $R = 50,000$ (a slit width of 0.72 arcsec), in October 2002 and May 2003. The atmospheric dispersion corrector (ADC) was used in all observing runs. Two EEV-CCDs were used with two by two on-chip binning, providing approximately a three-pixel

⁴ $[\text{A}/\text{B}] = \log(N_{\text{A}}/N_{\text{B}}) - \log(N_{\text{A}}/N_{\text{B}})_{\odot}$, and $\log \epsilon_{\text{A}} = \log(N_{\text{A}}/N_{\text{H}}) + 12$ for elements A and B.

sampling of the resolution element. The spectra obtained in October 2002 cover the wavelength range 4100–6850 Å, with a small gap in the coverage between 5440 and 5520 Å due to the physical separation between the two CCDs. The wavelength coverage was slightly (~ 70 Å) shifted to shorter wavelengths in the May 2003 run. For CS 29528–028, which is the hottest star in our sample, a blue spectrum (3550–5250 Å) was also obtained during the October 2002 run.

Spectra of several stars not listed in Table 1 were also obtained. These stars, however, turned out to exhibit severe molecular absorption (C_2 and CN), and special care is required for their abundance analysis. These spectra will be reported on separately (Goswami et al. 2006).

2.3. Red Spectra of Nine Additional Stars

Table 3 lists the object names and observing log for stars for which we have also provided an analysis of Na. All stars other than CS 22183–015 were studied by our previous work (Aoki et al. 2002c,d), based on blue spectra. CS 22183–015 was studied by Johnson & Bolte (2002) and Cohen et al. (2006), but the Na abundance was not measured by these authors.

Most of the red spectra were obtained with Subaru/HDS in 2005 during scheduled service observing. The single exception is CS 22898–027, which was observed during the HDS commissioning phase in 2000. Photon counts per 0.18 km s^{-1} pixel at 5900 Å are listed in Table 3. Note that although some objects were observed for the purpose of radial-velocity monitoring, the counts are sufficient for our present analysis.

2.4. Data Reduction

Standard data reduction procedures (bias subtraction, flat-fielding, background subtraction, extraction, and wavelength calibration) were carried out with the IRAF echelle package⁵. Suspected cosmic-ray hits are removed using the technique described by Aoki et al. (2005).

The sixth column of Table 1 lists the photon count (per 1.8 km s^{-1} pixel) collected at 5200 Å. Since the primary purpose of this work is to investigate the abundance characteristics for a large sample, we pursued only moderate signal-to-noise (S/N) ratios that could be obtained with relatively short integrations. Note also that the data quality is not uniform in our sample. One reason for this is that complete optical photometry was not available at the time of the spectroscopic observing run. Moreover, our sample consists of stars having quite different colors. These factors made the estimation of exposure times required to obtain uniform S/N ratios quite difficult.

⁵IRAF is distributed by the National Optical Astronomy Observatories, which is operated by the Association of Universities for Research in Astronomy, Inc. under cooperative agreement with the National Science Foundation.

2.5. Measurements of Equivalent Widths

Equivalent widths are measured for isolated atomic lines by fitting gaussian profiles, while a spectrum-synthesis technique is applied to molecular bands. The measured equivalent widths of a number of elements are listed in Tables 4, 5, and 6. We selected 10 elements (12 species) for the measurements of equivalent widths.

Table 7 lists the equivalent widths of lines in the blue range for CS 29528–028. As shown below, the heavy neutron-capture elements in this star are significantly overabundant, and equivalent widths of the Sr, Zr, La, Ce, and Nd lines are measured.

The equivalent widths of Na lines for the nine other stars are listed in Table 8. The Na D lines could not be measured for CS 31062–050 because of severe contamination from interstellar Na absorption. The Na abundance of this object is determined from the $\lambda 5688$ Å line.

2.6. Measurements of Radial Velocities

We measure heliocentric radial velocities (V_r) using isolated Fe I lines. The results are listed in Table 1. The standard error (σ/\sqrt{n} , where σ is the standard deviation of the values from individual lines and n is the number of lines used) is adopted as the random error of the measurements reported in the table. The wavelength calibration was made using Th-Ar comparison spectra that were obtained during the observing runs. Possible systematic errors of the wavelength calibration due to the stability of the spectrograph are no more than 0.4 km s^{-1} (see Aoki et al. 2005). Combining this possible systematic error with the random errors (3σ), the uncertainties of the reported radial velocity measurements are $0.5\text{--}1.0 \text{ km s}^{-1}$.

The V_r of BS 16929–005 measured in the present work agrees with that of Honda et al. (2004a) (-51.29 km s^{-1}) within the stated errors. No significant variation was found for this object between the two observations, taken roughly two years apart. The radial velocities and the binarity of CS 22948–027 and CS 29497–034 were investigated by Barbuy et al. (2005). Our results agree, within the measurement errors, with the predictions from the orbital parameters for these two stars derived by these authors. Different orbital parameters for CS 22948–027 were determined by Preston & Sneden (2001). Although the values of the orbital parameters are quite different between the two studies, both predict a similar velocity at the epoch of our observation. Hence, our measurement for a single epoch does not provide meaningful constraints on the determination of the orbital parameters for CS 22948–027 at present. Further monitoring of the radial velocity of this star is strongly desired.

3. Chemical Abundance Analyses and Results

A standard LTE analysis, employing the model atmospheres of Kurucz (1993), is performed for the measured equivalent widths for most of the detectable elements, while a spectrum-synthesis technique is applied for the CH, C₂, and CN molecular bands.

Since the calculations of model atmospheres used in the present analyses are made for scaled solar abundances, the effect of the enhancements of carbon and nitrogen on thermal structures is not included. This may have some affect on cool stars with large excesses of these elements. Hill et al. (2000) showed that the temperature at the layers where weak absorption lines form ($\log \tau = -1$ to 0) is a few hundred kelvin higher in the CN-enhanced ($[\text{C}/\text{Fe}] = [\text{N}/\text{Fe}] = +2$ for $[\text{Fe}/\text{H}] = -3$) model for $T_{\text{eff}}=4500$ K than in the standard model (that is, the model based on scaled solar abundances). The effect of the enhancements of carbon and nitrogen on, for instance, iron abundances derived from Fe I lines, might be 0.2–0.3 dex, which is estimated from the sensitivity of the derived abundances to the effective temperatures adopted for a few cool stars ($T_{\text{eff}} \lesssim 4500$ K) in our sample (e.g., HE 1447+0102). We note that the carbon enhancement of CS 30322–023, the coolest object in our sample, is relatively small ($[\text{C}/\text{Fe}] = +0.56$, see § 3.2), thus the effect of the carbon enhancement on the thermal structure of the model atmosphere for this star might be less significant.

3.1. Atmospheric Parameters

Effective temperatures are often determined in high-resolution spectroscopic studies by ensuring that the derived abundance of some species (e.g., Fe) is independent of the excitation potential of the spectral lines employed. However, since the measurement accuracy of the weak absorption lines is not so high in our moderate S/N spectra, the spectroscopic method to determine effective temperature is less than ideal. Instead, we estimate effective temperatures of our program stars from broad-band photometry, although we note that the determination of effective temperatures for CEMP stars from photometric data can also present a challenge, due to the presence of severe molecular absorption in some photometric bands.

We first estimate the effective temperatures for the stars in our sample from their $V-K$, $V-R$, $V-I$, and $R-I$ colors, using the empirical temperature scale of Alonso, Arribas, & Martínez-Roger (1996) for CS 29503–010 and CS 29528–028 (warm stars) and Alonso, Arribas, & Martínez-Roger (1999) for the others, after reddening corrections were applied (Table 2). Corrections for the filter systems which we employed, in order to put them onto the Alonso et al. scale, were as reported by Aoki et al. (2005). The metallicity applied to the effective temperature scale is first assumed to be $[\text{Fe}/\text{H}] = -2.5$, and is then corrected after the first-pass abundance analysis has been completed. The determination of the effective temperature and abundance analysis are iterated until the derived iron abundance is no longer significantly different from the assumed value. We give priority to the results from $V-K$ ($T_{\text{eff}}(V-K)$), as mentioned below, which are listed in Table 2. The average

of the effective temperatures from the other three colors is calculated, and the differences of this average with respect to $T_{\text{eff}}(V - K)$ are also listed in the Table. A typical error of the $V - K$ color is 0.03 mag (errors of the K -band photometry and reddening estimates are usually dominant). The error of the $(V - K)_0$ of 0.03 mag results in an uncertainty in T_{eff} of 90 K.

The effect of molecular absorption is relatively small in the V and K bands for most stars in our sample. Indeed, the $V - K$ colors calculated by models including enhancements of carbon and nitrogen by Hill et al. (2000) are in reasonable agreement with the values derived by the empirical color- T_{eff} relation by Alonso, Arribas, & Martínez-Roger (1999). For this reason the results from the $V - K$ color is adopted for most of our program stars. However, we made corrections to the effective temperatures of the following five stars:

(1) **CS 22948–027 and CS 29497–034:** These stars have been studied in previous work by Hill et al. (2000) and Barbuy et al. (2005), who adopted $T_{\text{eff}} = 4800$ K for both objects. The effective temperatures we derived from the $V - K$ colors are 330 K and 230 K higher than their values, respectively. These differences could be due to the differences in the reddening corrections adopted. Moreover, other colors yield lower temperatures. Including these results, we adopt 5000 K and 4900 K for CS 22948–027 and CS 29497–034, respectively, in our analysis.

(2) **HE 1005–1439 and HE 1447+0102:** A large discrepancy between $T_{\text{eff}}(V - K)$ and those estimated from the other three color indices is found in stars with strong C_2 and CN molecular bands; in general, the temperature derived from $V - K$ is lower (the effect of molecular bands on $R - I$ color is significant), as was also found for CS 22948–027 and CS 29497–034. However, the opposite results are obtained for HE 1005–1439 and HE 1447+0102, for which quite high temperatures are derived from the $V - K$ colors. We suspect there is some problem in the estimate of the temperatures from this color for these objects, and adopt the lower values.

(3) **CS 29528–028:** The effective temperature of CS 29528–028 from the $V - K$ and other colors is higher than the values found in most low-metallicity main-sequence turn-off stars. In such stars, the effect of molecular absorption is almost negligible in the broad-band photometry, and the $B - V$ color also provides useful information. The effective temperature of CS 29528–028 from the $B - V$ calibration (Alonso, Arribas, & Martínez-Roger 1996) is 6580 K, significantly lower than that from $V - K$. We adopted 6800 K for this object.

For the above five stars we assumed larger uncertainties in the estimate of errors of abundance determination due to the uncertainties in their adopted atmospheric parameters (see § 3.4).

We perform an abundance analyses of our program stars in the standard manner for the measured equivalent widths of Fe I and Fe II lines. The microturbulent velocity (v_{turb}) is determined from the Fe I lines by demanding that there exist no dependence of the derived abundance on equivalent widths. For HE 0507–1653, HE 1157–0518, HE 1319–1935, and HE 2221–0453, however, no or only a few weak Fe I lines were available, hence reliable microturbulent velocities could not be directly determined. In these cases we assumed a microturbulent velocity of 2.0 km s^{-1} , close to the average of the values of the other CEMP giants in our sample. A larger uncertainty on the

microturbulent velocity is assumed for these three stars in calculations of their abundance errors (§ 3.4).

Surface gravities ($\log g$) are determined from the ionization balance between Fe I and Fe II. The final atmospheric parameters are reported in Table 9. Figure 1 shows the correlation between the effective temperatures and gravities for our sample (filled circles) and also for other stars studied by previous work (see §3.6 for references). A clear correlation is found for stars with $T_{\text{eff}} < 5500$ K, as most stars in our sample lie along the halo red-giant branch. Our sample also includes a number of main-sequence turn-off and subgiant stars.

We investigated the correlation between the lower excitation potential and the derived Fe abundances from individual Fe I lines. We found that eight objects among the 26 stars show statistically significant dependence of the derived abundances on the excitation potential. The dependence disappears by assuming lower effective temperatures by 150–250 K than derived from the colors. This result possibly implies that our calibration based on color indices systematically overestimates the effective temperature of CEMP stars. However, given the agreement of the results for similar number of objects for which sufficient number of Fe I lines are measured, the systematic error is unlikely to be as large as 200 K. It should be noted that the five objects to which we applied special corrections of effective temperatures show no significant correlation between the excitation potential and the abundances from individual Fe I lines.

For the stars for which Na abundance measurements are made, we adopt the atmospheric parameters determined by Aoki et al. (2002c), Cohen et al. (2006), and Aoki et al. (2002d) for CS 22957–027, for CS 22183–015, and for the other seven stars, respectively.

3.2. Carbon and Nitrogen Abundances

For the CH 4323 Å band and/or the C₂ Swan bands, carbon abundances are determined using a spectrum-synthesis approach. The CH band is used for stars that have relatively weak absorption features of molecules due to their high temperature and/or small excesses of carbon. The C₂ Swan 0–0 band (5167 Å) is applied to the analysis for stars in which the CH band is highly saturated. For cool objects with significant enhancements of carbon, even the C₂ Swan 0–0 band is severely saturated. In these instances the C₂ Swan 0–1 band at 5635 Å is used. The results are listed in Table 10, where the absorption band used for the analysis is also presented for each star. There exist some uncertainties in the transition probabilities of these molecular bands, which may possibly cause systematic errors in the carbon abundance determinations. The abundance analysis for the CEMP subgiant LP 625–44 by Aoki et al. (2002a), using these same three bands, and for which the same line lists as those used in the present study were adopted, demonstrated that the derived carbon abundance from the C₂ bands is 0.2 dex higher than that from the CH band. Thus, a small systematic error in the carbon abundance determination possibly exists, depending on the molecular bands applied to the analysis.

The carbon isotope ratio ($^{12}\text{C}/^{13}\text{C}$) is measured using the C_2 Swan 1–0 bands at 4736 Å ($^{12}\text{C}_2$) and 4745 Å ($^{12}\text{C}^{13}\text{C}$) for 12 objects in which these bands are detected. The line list and analysis technique used by Aoki & Tsuji (1997) are adopted. The results are listed in Table 11. Most stars have $^{12}\text{C}/^{13}\text{C}$ ratios around 10, a typical value found in classical CH stars (e.g., Aoki & Tsuji 1997), while quite high values of this ratio are found for three of our program stars.

The nitrogen abundances are estimated from the CN 4215 Å band. For some of our stars the band appears clearly, and without severe saturation. In these cases, a reliable fit of synthetic spectra to the observed one is obtained. However, this band is not detected in seven of our program stars, and only upper limits on nitrogen abundances are determined (see Table 10). For some cool objects the CN band is so severely saturated that the fitting of the synthetic spectra is quite uncertain. We compare the observed spectrum and the synthetic ones calculated changing the nitrogen abundances, and estimate the fitting errors by eye. In the worst case the uncertainty reaches 0.5 dex.

3.3. Other Elements

The abundances of other elements are measured by standard analyses for the measured equivalent widths. The effects of hyperfine splitting on abundance determination are significant in the analysis of Ba lines if the abundances of isotopes with odd mass numbers (^{135}Ba and ^{137}Ba) are high (McWilliam 1998). This is the case when the contribution of the r-process is large, while the s-process mostly yields ^{138}Ba . Hence, the derived abundances are dependent on the processes of Ba production that are assumed in the analysis.

We first determine the Ba abundances with a single-line approximation, and classify our sample into “Ba-enhanced” and “Ba-normal” stars. Here, a Ba-enhanced star is defined as having $[\text{Ba}/\text{Fe}] > +0.5$ (see § 5.1). For Ba-enhanced CEMP stars, we assume that the origin of barium is the s-process, and re-calculate the abundances including hyperfine splitting, assuming the Ba isotope ratios estimated by Arlandini et al. (1999).⁶ The effect of hyperfine splitting on the abundances derived from the two resonance lines is on the order of 0.1 dex or smaller. For Ba-normal stars, we assume the Ba isotope ratios of the r-process component in solar-system material, and derive the final abundance including the effects of hyperfine splitting. The result of including hyperfine splitting is 0.1–0.2 dex, depending on the strengths of the Ba lines.

For CS 29528–028, for which a blue spectrum was obtained in the present study, the abundances of neutron-capture elements other than Ba are measured (Table 12). The effect of hyperfine splitting is included in the analysis of La lines, using the line data by Lawler et al. (2001). The over-

⁶This assumption is invalid for CEMP stars with excesses of r-process elements like CS 22892–052 (Snedden et al. 1996). Such objects are, however, known to be very rare (e.g., Beers & Christlieb 2005), although the abundances of r-process elements are not determined in the present analysis.

abundances of the heavy neutron-capture elements (Ba–Nd) are extremely high, while the excesses of the light neutron-capture elements (Sr and Zr) are relatively small. This abundance pattern is similar to those found in other CEMP stars with excesses of s-process elements (e.g., Aoki et al. 2002d).

Sodium abundances are determined for 30 stars, including nine objects for which abundances of other elements were previously studied, using the D lines ($\lambda\lambda 5889$ Å, 5895 Å) for most of the stars with available red spectra. These lines are known to be significantly affected by non-LTE effects. The abundances derived from these lines are corrected for these effects using the results of Takeda et al. (2003), who provide the non-LTE corrections for the 5895 Å line in their Figure 2. We assume the same corrections apply to the 5889 Å line.

Table 13 presents the results of the Na abundance measurements. The results of an LTE analysis are listed in the third column, while the non-LTE corrections applied to the results from the D lines, which are dependent on the line strength, are listed in the fourth column. For several stars, the subordinate lines at 5682 Å and 5688 Å are used to measure the Na abundances. The non-LTE effects on these weak lines are estimated to be quite small (Takeda et al. 2003). The final results are obtained from the non-LTE corrected Na abundances from the D lines and LTE results from the subordinate lines, and are listed in the fifth and sixth columns of Table 13. The Na abundances of four stars are determined using all four of these lines. For CS 29528–028 and HE 0400–2030, the non-LTE corrected values derived from the D lines agree well with the results from the subordinate lines. However, for CS 22957–027, the results from the D lines are higher by 0.5 dex than those from the other lines, even though a large non-LTE correction (0.5 dex) is applied to the results from the D lines. By contrast, for HE 0507–1653, the results from the subordinate lines are higher by 0.3 dex than the non-LTE corrected values from the D lines. These discrepancies imply that either (1) the non-LTE corrections applied to these stars are inappropriate, or (2) measurements of LTE abundances from the very strong D lines and/or very weak subordinate lines are uncertain. We note, however, that the abundances derived from the two subordinate lines agree well in CS 22957–027 and HE 0507–1653. This suggests that either errors exist in the abundance measurements for the D lines, or in the non-LTE corrections, or in both.

3.4. Uncertainties

The random errors in abundance measurements obtained from analysis of molecular bands are estimated by fitting with synthetic spectra calculated by changing the assumed abundances of carbon and nitrogen, as mentioned in § 3.2. Random abundance errors in the analysis are estimated from the standard error of the abundances for each species. These values are sometimes unrealistically small, however, when only a few lines are detected. For this reason, we adopted the larger of (1) the value for the listed species, or (2) the standard error derived using the standard deviation of the abundance from individual Fe I lines and the number of lines used for the species as estimates of the random errors. Typical random errors are on the order of 0.1–0.15 dex.

Errors arising from uncertainties in the atmospheric parameters are evaluated by adopting $\sigma(T_{\text{eff}}) = 100$ K, $\sigma(\log g) = 0.3$ dex, and $\sigma(v_{\text{tur}}) = 0.3$ km s⁻¹ for four stars, taking the evolutionary status and strength of the molecular bands into consideration: CS 22174–007, a giant with relatively weak molecular absorption; CS 22948–027, a giant with strong molecular absorption; CS 30322–023, a cool giant; and CS 29503–010, a main-sequence star. The uncertainties estimated for each of our program stars are taken to be equal to those associated with the one of these four templates that is closest in evolutionary status and in strength of the molecular bands. For stars whose effective temperatures are more uncertain (see § 3.1) the abundance uncertainties are estimated assuming $\sigma(T_{\text{eff}}) = 200$ K. For stars for which the microturbulent velocities are assumed to be 2.0 km s⁻¹, $\sigma(v_{\text{tur}}) = 0.6$ km s⁻¹ is assumed in obtaining estimates of abundance uncertainties. Finally, we derive the total uncertainty by adding, in quadrature, the individual errors, and list them in Table 10.

The above error estimates do not include possible systematic errors arising from non-LTE effects. The non-LTE correction for iron abundances is on the order of +0.2 dex in very metal-poor stars, according to Thévenin & Idiart (1999), although Gratton et al. (1999) find no strong effects (< 0.1 dex) for dwarfs and red giants cooler than 5000 K. The effect on the abundance ratios of important elements in this work (e.g. Ba, Mg) is also 0.1–0.2 dex, depending on the spectral lines used for the analyses (Asplund 2005).

The effects of inhomogeneity of the stellar atmosphere (the so-called 3D effects) are also thought to have a significant influence on the determination of C and N abundances from molecular features (Asplund 2005). Although quantitative estimates for 3D effects, coupling with non-LTE ones, are not available at present, the corrections are possibly on the order of 0.5 dex or more (in the negative direction). We do not apply any correction for these effects in this paper. Instead, we compare below our results with other studies that derived carbon and nitrogen abundances from molecular bands for carbon-enhanced and non carbon-enhanced stars.

3.5. Comparison with Previous Work

The chemical composition of the extremely metal-poor ([Fe/H] = −3.1) star BS 16929–005 was determined by Honda et al. (2004b). Although the wavelength coverage is different between their study and ours, the results for elements analyzed in common agree to within 0.15 dex. An exception is Ca, for which our analysis yields a [Ca/Fe] lower by 0.3 dex. There is no Ca I line analyzed in common by the two studies. Our measurement is based on only two lines, at 4226 Å and 6162 Å. Magain (1988) and Ryan, Norris & Beers (1996) found the first of these lines yields abundances that are systematically lower than other Ca I lines by 0.18 dex. Similar results are found for CS 30312–100, which has similar stellar parameters to BS 16929–005, and for which the Ca abundance is determined from 10 Ca I lines, including the two mentioned above. The abundances derived from the lines at 4226 Å and 6162 Å are 0.1 dex lower than the average of the result provided by the other available Ca I lines. Given this, and the small number of lines

measured by the present analysis (two lines), the discrepancy of 0.3 dex is possibly a result of random errors.

Two stars from our program with very large carbon enhancements, CS 22948–027 ($[\text{C}/\text{Fe}] = +2.1$) and CS 29497–034 ($[\text{C}/\text{Fe}] = +2.7$), have been studied in detail by Hill et al. (2000) and, more recently, by Barbuy et al. (2005). Here we compare our results with those reported by Barbuy et al. (2005). The iron and carbon abundances of CS 22948–027 derived by our present analysis are about 0.2 dex higher than theirs. This result is well explained by the difference of effective temperatures adopted in the analyses (our effective temperature is 200 K higher). The nitrogen abundance determined by our study is significantly (about 0.7 dex) higher than theirs. This could also, at least in part, be explained by the difference in the atmospheric parameters adopted by the two studies. Note that Barbuy et al. (2005) used CN lines of the red system for the abundance analysis, while we analyze a band of the CN violet system, which could also contribute to the discrepancy in the derived N abundances. Our Na abundance is also 0.35 dex higher than their LTE abundance determination for this element. The abundances of other elements studied by both works show fairly good agreement.

For CS 29497–034, the results of our study agree well with those of Barbuy et al. (2005). The exceptions are for Na and Mg, for which we derive abundances that are 0.4 and 0.5 dex higher for these elements, respectively. The small differences in the atmospheric parameters adopted by the two studies cannot explain these discrepancies. The abundances of these two elements for CS 29497–034, as well as the Na abundance for CS 22948–027, are determined from only two very strong lines, and small measurement errors in equivalent widths could result in large abundance errors. We note, however, that the excesses of Na and Mg in CS 29497–034 are clearly found in the results of Barbuy et al. (2005), as well as in our analysis.

3.6. An extended sample of CEMP stars

For the following discussion we combined the results of recent abundance studies for CEMP stars (Preston & Sneden 2001; Aoki et al. 2002a,b,c,d; Depagne et al. 2002; Cohen et al. 2003; Lucatello et al. 2003; Aoki et al. 2004; Cohen et al. 2004; Barklem et al. 2005; Ivans et al. 2005; Tsangarides 2005; Cohen et al. 2006; Jonsell et al. 2006) with those of the present work. A total of 42 stars, including nine for which Na abundances are determined by our analysis, are compiled. It should be noted that, although CS 22892–052 is an CEMP star having a large Ba overabundance, the origin should be quite different from that for other Ba-enhanced CEMP stars. Hence, this object is not included in our sample. Details of the selection of the results for objects for which more than one paper reported chemical abundances are discussed in the Appendix. The chemical composition and atmospheric parameters for the extended sample of CEMP stars (64 objects, including 22 stars studied by the present work) are listed in Table 14.

4. Carbon Abundance Ratios and a Revised Definition of CEMP stars

Figure 3 shows the carbon abundance ratios ($[C/Fe]$) as a function of iron abundances ($[Fe/H]$) for our sample (filled circles) and for other CEMP stars studied by previous work (filled squares). The carbon abundances of these stars are determined from the strengths of the molecular bands of CH and/or C_2 . The carbon abundances for other stars that were not regarded as carbon-enhanced objects by previous studies are indicated with crosses (Gratton et al. 2000; Cayrel et al. 2004; Honda et al. 2004b; Aoki et al. 2005). The carbon abundances for these stars were measured from the CH band. We caution that Figure 3 cannot be used to constrain the fraction of CEMP stars as compared to other metal-poor stars, because of bias in the sample selection. Lucatello et al. (2006) provides a discussion of these phenomena based on a sample with better-controlled selection criteria (the HERES sample of Barklem et al. 2005).

Our program stars distribute in metallicity from $[Fe/H] = -1$ to -3.3 , providing a useful sample to investigate the metallicity dependence of the abundance trends of CEMP stars. There are 21 stars in our sample with remarkable excesses of carbon ($[C/Fe] > +1$), while the $[C/Fe]$ values of the five other newly-analyzed stars are not clearly distinguishable from most stars which were *not* identified as carbon-enhanced objects by previous work. Before proceeding with our inspection of elemental abundance patterns, we first consider an appropriate definition for the carbon-enhancement phenomenon in metal-poor stars.

The carbon abundance at the surface of a star is expected to decrease when the star evolves to become a red giant, due to mixing with internal material that has been affected by the CNO cycle (the first dredge-up). A further decrease of carbon, accompanied with an increase of nitrogen, has been observed in highly evolved metal-poor red giants (e.g., Spite et al. 2005), indicating the influence of extra mixing during evolution along the red-giant branch (Charbonnel 1995). As a result, the surface abundance of carbon in late-type stars will in general be lower than it was when the star was in an earlier evolutionary stage. These evolutionary effects should thus be included in the definition of CEMP stars.

For this purpose we calculate the luminosities of the stars in our present sample, and for other stars studied by previous work, using the relation

$$L/L_{\odot} \propto (R/R_{\odot})^2 (T_{\text{eff}}/T_{\text{eff}\odot})^4 \propto (M/M_{\odot})(g/g_{\odot})^{-1} (T_{\text{eff}}/T_{\text{eff}\odot})^4,$$

assuming the mass of the stars to be $0.8 M_{\odot}$, following Aoki et al. (2005) and Ryan et al. (2005). Figure 4 depicts $[C/Fe]$ as a function of luminosity. The $[C/Fe]$ values of most stars studied in previous works are around $+0.4$ for $\log(L/L_{\odot}) \lesssim 2.5$, while the value decreases with increasing luminosity. A similar trend was obtained by Gratton et al. (2000) for their metal-poor field giants (Figure 10 of their paper). We note that their carbon abundance ratios ($[C/Fe]$) are systematically lower than ours by about 0.4 dex, although their abundances were determined from the CH molecular bands as in our present analyses. This discrepancy might arise because of the difference in the metallicity ranges studied: the Gratton et al. sample mostly consists of stars with $[Fe/H]$

> -2 , while the non carbon-enhanced stars shown in Figure 4 have $[\text{Fe}/\text{H}] \lesssim -2.5$. The difference of metallicity could result in differences in the intrinsic carbon abundances, or in a difference in the 3D effects in stellar atmospheres. Gratton et al. (2000) also found decreases in $[\text{Li}/\text{H}]$, $^{12}\text{C}/^{13}\text{C}$, and an increase in $[\text{N}/\text{Fe}]$, at $\log(L/L_\odot) > 2$, which are expected to accompany a decrease of carbon during evolution along the red-giant branch. We note that some systematic errors possibly exist in our estimates of luminosity (e.g., NLTE effects on the determination of surface gravities) and also in carbon abundances (e.g., 3D effects on the molecular bands). However, such systematic errors do not directly affect the empirical definition of CEMP stars adopted here.

From inspection of Figure 4 we define the stars that satisfy the following criteria as CEMP stars:

1. $[\text{C}/\text{Fe}] \geq +0.7$ for stars with $\log(L/L_\odot) \leq 2.3$
2. $[\text{C}/\text{Fe}] \geq +3.0 - \log(L/L_\odot)$ for stars with $\log(L/L_\odot) > 2.3$

The division between CEMP and non-CEMP stars, using the above definition, is indicated by the dotted line in Figure 4. Four stars with $[\text{C}/\text{Fe}] < +0.7$ (CS 22174–007, CS 22886–042, CS 30312–100, and CS 31062–041) are consequently dropped from the sample of CEMP stars. On the other hand, the cool giant CS 30322–023 ($\log(L/L_\odot)=2.9$) is included in the sample of CEMP stars, although its $[\text{C}/\text{Fe}]$ value is only $+0.56$. Another example of a cool giant with relatively low $[\text{C}/\text{Fe}]$ that meets our revised definition of CEMP stars is CS 30314–067 ($[\text{C}/\text{Fe}]=+0.5$ and $\log(L/L_\odot)=3.2$), which was studied by Aoki et al. (2002b). Both cool giants have quite high nitrogen abundances ($[\text{N}/\text{Fe}] = +2.5$ and $+1.2$ for CS 30322–023 and CS 30314–067, respectively), suggesting that a significant amount of carbon was converted to nitrogen during their red-giant evolution.

With the application of the above criteria, a total of 22 stars in our sample are classified as CEMP stars. The following discussion is based on these 22 stars and 42 additional stars studied in previous work (shown by filled squares in Figure 4) that meet our revised definition of CEMP stars. It should be noted that Figure 3 shows that there is an approximate limit to the observed $[\text{C}/\text{Fe}]$ values at a given metallicity. The limit corresponds to $[\text{C}/\text{H}] \sim 0$. This point is discussed in more detail in § 5.2.

5. Discussion

5.1. Barium Abundance Ratios

Barium is a key element for identifying the origin of carbon in CEMP stars (see § 1). Ryan et al. (2005) separated their sample of CEMP stars into two groups of Ba-enhanced and Ba-normal stars. Figure 5 shows the barium abundance ratio ($[\text{Ba}/\text{Fe}]$) as a function of $[\text{Fe}/\text{H}]$ for our expanded sample. A large scatter of barium abundances is known to exist for very metal-deficient stars (e.g.,

McWilliam 1998; Honda et al. 2004b). However, stars with $[\text{Ba}/\text{Fe}] > +0.5$ are quite rare among non carbon-enhanced objects. Here we define stars with $[\text{Ba}/\text{Fe}] > +0.5$ as “Ba-enhanced” objects, following Ryan et al. (2005)⁷. In Figure 5 the four stars that are excluded from our sample of CEMP stars are shown by open circles – the barium abundances of these stars are normal.

One clear result seen from inspection of Figure 5 is that 36 of the 37 CEMP stars with $[\text{Fe}/\text{H}] \geq -2.6$ are Ba-enhanced objects. The exception is HE 1410+0213 (Cohen et al. 2006). The iron abundance of this star, determined from Fe I lines, is $[\text{Fe}/\text{H}] = -2.16$. However, note that the $[\text{Fe}/\text{H}]$ derived from Fe II lines for this object is 0.41 dex lower than that from Fe I. Thus, the iron abundance of this star is possibly lower than that shown in the Figure, and closer to $[\text{Fe}/\text{H}] = -2.6$. Our first conclusion is that a majority of, if not all, CEMP stars with relatively high metallicity ($[\text{Fe}/\text{H}] \geq -2.6$) also exhibit excesses of the neutron-capture element Ba.

The $[\text{Ba}/\text{Fe}]$ abundance ratios for the stars in our expanded sample are shown as a function of $[\text{C}/\text{Fe}]$ in Figure 6 (the upper panel). A correlation between the barium and carbon abundance ratios is seen for the Ba-enhanced stars. The solid line in this Figure indicates the correlation for stars with $[\text{Ba}/\text{Fe}] > +0.5$ (54 stars). The null hypothesis that there is no correlation between the two values is rejected by the regression analysis, as well as by the Spearman rank correlation test, at the 99.9% confidence level. This suggests that the excesses of both the barium and carbon originate in the same astrophysical site, which is most likely to be AGB progenitor stars.

As noted above, the carbon abundances of giants are possibly affected by internal processes, including the CN-cycle. The total abundance of carbon and nitrogen might thus better represent the initial enrichment of carbon by progenitor objects. For this purpose, we also show $[\text{Ba}/\text{Fe}]$ as a function of $[(\text{C}+\text{N})/\text{Fe}]$ in the lower panel of Figure 6. As described above, the CN band is not detected in seven stars, and only upper limits on nitrogen abundances are determined. For these stars the upper limit of $[(\text{C}+\text{N})/\text{Fe}]$ is determined by adopting the upper limit of the nitrogen abundance, while the lower limit of $[(\text{C}+\text{N})/\text{Fe}]$ is determined by assuming the nitrogen abundance to be zero. The values are listed in Table 11.

The correlation between $[\text{Ba}/\text{Fe}]$ and $[(\text{C}+\text{N})/\text{Fe}]$ of 44 objects for which $[(\text{C}+\text{N})/\text{Fe}]$ values are determined is shown by the dashed line in the Figure. Although the correlation appears weaker than that found for the $[\text{C}/\text{Fe}]$ case, the significance level of the rejection of the no-correlation null hypothesis is still as high as 99%. The reason for the somewhat weaker correlation is the existence of strongly N-enhanced stars among very metal-poor objects (e.g. CS 22960–053, CS30322–023). Here we separate the sample into two groups with $[\text{Fe}/\text{H}] \geq -2.6$ (29 objects) and $[\text{Fe}/\text{H}] < -2.6$ (15 objects). In Figure 6, stars with $[\text{Fe}/\text{H}] < -2.6$ are shown by symbols with open circles, and the correlation is exhibited by the solid line. A clear correlation between $[(\text{C}+\text{N})/\text{Fe}]$ and $[\text{Ba}/\text{Fe}]$ is seen for stars with higher metallicity, confirming the above suggestion of the correlation between

⁷Note that Beers & Christlieb (2005) adopted a somewhat different criterion in their definition of CEMP-no stars ($[\text{Ba}/\text{Fe}] < 0$) vs. CEMP-s stars ($[\text{Ba}/\text{Fe}] > +1.0$; $[\text{Ba}/\text{Eu}] > +0.5$).

[Ba/Fe] and [C/Fe]. The slope of the solid line (0.84 dex per dex) is also interesting. If the [Ba/Fe] and [C/Fe] values are determined by the enrichment of AGB stars and the dilution in the secondary objects, a slope of unity is expected. The regression analysis indicates that this possibility cannot not be rejected (at the 70% confidence level). A discussion of the stars with lower metallicity can be found below.

As can be seen in Figure 5, the 27 stars with $[\text{Fe}/\text{H}] < -2.6$ exhibit a large range of Ba abundances ($-1.2 < [\text{Ba}/\text{Fe}] < +3.3$).⁸ Nine of them are Ba-normal stars according to our definition. Figure 7 shows the [Fe/H] distribution for Ba-enhanced and Ba-normal CEMP stars, respectively. The Ba-normal stars are only found in the lowest metallicity range, while Ba-enhanced stars are distributed over a range in [Fe/H] above -3.3 . The null hypothesis that the samples are drawn from the same parent populations in [Fe/H] is rejected by the rank-sum (Mann-Whitney) test at the 99.9% confidence level. Our second conclusion is thus that some source(s) of carbon enhancement that are different from “standard” AGB nucleosynthesis must operate efficiently at low metallicity.

In the smaller sample discussed by Ryan et al. (2005), CEMP stars are clearly distinguished into two groups according to their barium abundances. However, Figure 5 shows that the CEMP stars with $[\text{Fe}/\text{H}] \sim -3$ rather exhibit a continuous distribution in barium abundances, owing partly to the two CEMP stars having $+0.6 \leq [\text{Ba}/\text{Fe}] \leq +1.0$ added by the present work (CS 22960–053 and CS 30322–023). These two stars have very high nitrogen abundance ratios, and their values of [Ba/Fe] and [(C+N)/Fe] deviate from the correlation found for stars with higher metallicity (Figure 6). Further observations of stars in this metallicity range are clearly desirable, in order to derive some more definitive conclusion on the distribution of Ba abundance ratios at the lowest metallicity.

5.2. Distribution of Carbon Abundances

As discussed in § 4, a limit on the carbon excess is seen in the distribution of carbon abundance ratios (Figure 3). This is more clearly seen in Figure 8, where the distributions of carbon abundances ([C/H]) are shown for Ba-enhanced and Ba-normal stars separately. Most of the Ba-enhanced stars have $-1 < [\text{C}/\text{H}] < 0$, and there is a cutoff of [C/H] values at around zero (i.e., solar abundance). We note that the four stars having $[\text{C}/\text{H}] > 0$ are CS 29503–010, HE 0206–1916, HE 1447+0102, and CS 22887–048. The [C/H] values of these stars are, however, at most +0.14 (see Table 14), and hence close to solar. Cohen et al. (2006) recently stated that the carbon abundances of their sample of CEMP stars are approximately constant at about 1/5th of the solar value. Most Ba-enhanced CEMP stars in our sample have carbon abundances that are higher than this value. However, their

⁸The three stars with the lowest iron abundances, HE 1327–2326 (Frebel et al. 2005), HE 0107–5240 (Christlieb et al. 2002), and G77–61 (Plez & Cohen 2005), are depicted in some of our Figures, but are not included in the statistics described in this paper.

sample includes Ba-normal CEMP stars, which could reduce the average of the carbon abundances. Given this point, and the relatively small sample size of Cohen et al. (2006), the distribution of carbon abundances derived here is compatible with their conclusion.

The enhancement of carbon in the Ba-enhanced CEMP stars is primarily determined by the process of AGB nucleosynthesis in the binary mass-transfer scenario. The material containing enhanced carbon is transferred to the surface of the companion, and is expected to be diluted during the evolution of the companion star by mixing with non-polluted material from the companion’s interior. Model calculations for the nucleosynthesis in AGB stars at low metallicity have shown that the final predicted yield of carbon is on the order of $[C/H] = 0$. For instance, van den Hoek & Groenewegen (1997) provide the total yields of CNO isotopes in their Table 5. The ^{12}C yields in mass are predicted to be $2.81\text{--}4.95 \times 10^{-3} M_{\odot}$, which corresponds to $[C/H] = -0.02 - +0.23$, for stars with initial mass in the range $1.3\text{--}3.0 M_{\odot}$ and metallicity of $Z = 0.001$ ($[\text{Fe}/H] = -1.2$). Ventura et al. (2002) derive a similar value ($[C/H] = -0.14$) for a star with $2.5 M_{\odot}$ and $Z = 0.0002$ ($[\text{Fe}/H] = -1.9$). The chemical compositions of the Ba-enhanced CEMP stars presumably represent the yields of such low-mass, metal-poor AGB stars. We note that the carbon yields rapidly decrease with increasing mass ($M \gtrsim 3M_{\odot}$), due to hot bottom burning.

Given these model yields of $[C/H] \sim 0$, the simplest explanation of the upper cutoff of $[C/H] \sim 0$ in Figures 3 and 8 is that the observed upper envelope represents objects in which the bulk of the material originated in the AGB star and was transferred when the secondary was on or near the main sequence. The amount of mass transferred was so large that subsequent mixing/dilution in the convection envelope of these objects during giant branch evolution has not greatly changed $[C/H]$ from the value that existed in material transferred from the AGB donor.

Although the $[C/H]$ values of most Ba-enhanced CEMP stars are found in a rather narrow range, a correlation between the $[C/H]$ and luminosity is found. The top panel of Figure 9 shows $[C/H]$ as a function of luminosity for the Ba-enhanced CEMP stars (filled symbols) and the Ba-normal ones (open symbols). A least-square fit to the data for the Ba-enhanced stars is shown by the solid line. The null hypothesis that no correlation exists between these two quantities is rejected by the regression analysis and by the Spearman rank correlation test, both at the 99.9% confidence level. The $[C/H]$ value decreases by 0.6 dex (i.e., a factor of four) with increasing luminosity from $\log(L/L_{\odot}) \sim 0$ to 3. If this correlation reflects the decrease of carbon abundance at the surface of the object during evolution along the red giant branch, two mechanisms to decrease carbon might be considered. One is the dilution of the carbon-rich material provided by the donor AGB star with the non carbon-rich material of the secondary we are currently observing. The other is the CN cycle inside the star through the first dredge-up and extra mixing. However, the bottom panels of Figure 9 exhibits a similar correlation between the $[(C+N)/H]$ values and luminosity to that found for $[C/H]$, although the confidence level of the null-hypothesis rejection is only 90% in this case. That is, the CN cycle is unlikely the primary reason for the relatively low carbon abundances found in some high luminosity objects. An exception is CS 30322–023 ($[C/H] = -2.69$ and $[(C+N)/\text{Fe}] = -1.46$), whose surface chemical composition should be severely affected by the CN cycle. We

also shows the plot for $[N/H]$ in the middle panel for completeness, where no statistically significant correlation is found between the two values.

In summary, some dilution of the envelope material in the receiving companion is suggested for Ba-enhanced CEMP stars from the correlation between $[C/H]$ (and $[(C+N)/H]$) and luminosity. Most Ba-enhanced CEMP stars in our sample show, however, that the decrease of $[C/H]$ during the stellar evolution is less than 1 dex. Given the fact that the convective layer becomes about two orders of magnitude deeper when a star evolves to become a red giant, the small dilution of carbon found in Ba-enhanced CEMP stars suggests that a significant amount of carbon-enhanced material has been accreted from the donor AGB star.

In contrast to the Ba-enhanced objects, the $[C/H]$ values of Ba-normal CEMP stars exhibit a very wide distribution, with an average value of $[C/H]$ that is significantly lower than that of Ba-enhanced stars. The difference of the $[C/H]$ distributions between the two groups are clearly seen in Figure 8. The null hypothesis that the samples are drawn from the same parent populations in $[C/H]$ is rejected by the rank-sum test at the 99.9% confidence level. This result suggests again a difference in the mechanisms that enrich carbon between Ba-normal and Ba-enhanced stars. We note that, since the average metallicity of Ba-normal CEMP stars is much lower than that of Ba-enhanced stars (Fig. 7), their carbon abundance ratios ($[C/Fe]$) are higher than the criterion for CEMP stars (§4), although their $[C/H]$ values are not outstandingly high. We also note that apparent correlations are found between the luminosity and abundance distributions of C, N, and C+N for Ba-normal stars in Figure 9. However, they are likely affected by observational bias. This issue is discussed further in the next subsection.

5.3. Evolutionary Status

Ryan et al. (2005) suggested that a difference exists in the evolutionary stages between the Ba-enhanced and Ba-normal CEMP stars. In their sample, the Ba-normal CEMP stars are found only at the top of the giant branch, while Ba-enhanced stars are found throughout the H-R diagram. The excess of unevolved Ba-enhanced CEMP stars, relative to Ba-normal ones, was attributed by Ryan et al. (2005) to the dilution of surface carbon enhancements in the Ba-enhanced stars during the evolution from the main-sequence to the red giant branch.

To examine this hypothesis for our expanded sample of CEMP stars, Figure 10 shows the luminosity distribution of Ba-enhanced and Ba-normal CEMP stars, respectively (see also Table 14). The luminosity, as estimated from our adopted atmospheric parameters as mentioned in §4, is an indicator of the stars' present evolutionary status. The Ba-enhanced stars distribute over a wide range of luminosity. We note that the number of objects at $\log(L/L_\odot) = 1\text{--}1.5$ is relatively small. This probably corresponds to the gap between giants and subgiant/main-sequence stars. Although no Ba-normal CEMP main-sequence star was included in our previous sample (Ryan et al. 2005), two such stars were reported by Cohen et al. (2004) and Cohen et al. (2006).

The suggested difference in the luminosity distributions between the Ba-enhanced and Ba-normal CEMP stars is not clear for the present sample. Indeed, according to the rank-sum test the difference of the luminosity distributions between these two groups shown in Figure 10 is not statistically significant (the null hypothesis of identical luminosity distributions for the two samples can be rejected at only the 46% significance level). Thus, the existence of different luminosity distributions for the Ba-enhanced and Ba-normal CEMP stars suggested by Ryan et al. (2005) is not confirmed by our expanded sample. Moreover, as discussed in § 5.2, the carbon abundance distribution of Ba-enhanced CEMP stars (Figure 8) shows a concentration around $[C/H] > -1$, regardless of evolutionary status, indicating that the dilution of the transferred material with carbon enhancement is not as significant as Ryan et al. (2005) presumed.

It should be kept in mind that the luminosity distribution of observed CEMP stars could be affected by a selection bias, because the strengths of the molecular bands are dependent on the stellar temperature, and, therefore, on the luminosity of the star. Figure 11 shows the $[C/H]$ values as a function of effective temperature. In this Figure the Ba-normal and Ba-enhanced stars are indicated by open and filled symbols, respectively. All Ba-enhanced stars but one (CS 30322–023) have $[C/H] \gtrsim -1$, while most of Ba-normal stars have lower carbon abundances. The CH bands that are used in the usual abundance studies are easily detected even in main-sequence stars if the carbon abundance is as high as solar (i.e., $[C/H] \sim 0$). However, if the abundance is lower than $[C/H] \sim -1.5$, quite high-quality spectra are required for detection of the CH band. In order to estimate the detection limit of the CH G band, we calculate synthetic spectra for model atmospheres of dwarfs ($T_{\text{eff}}=6000\text{--}7000$ K and $\log g=4.0$), subgiants ($T_{\text{eff}}=5500$ K and $\log g=3.5$) and giants ($T_{\text{eff}}=4000\text{--}5000$ K and $\log g=1.0\text{--}2.5$). The dotted line in Figure 11 indicates the $[C/H]$ values required for the depth of the CH G band to be about 2 %, which we take as a conservative limit for detection of this feature in high-quality high-resolution spectra. The detection limit of the CH G band in medium-resolution spectra, by which CEMP stars are usually initially identified in surveys, is higher than the values shown by this line⁹. Even if Ba-normal CEMP main-sequence stars having similar carbon excesses to those found in Ba-normal CEMP giants exist, they would not be identified as CEMP stars in the surveys. On the other hand, carbon-enhanced giants are detected even if the carbon enhancement is not as significant as those of CEMP main-sequence stars. Ba-enhanced dwarfs as well as giants are detected because of their very high carbon excesses. This could lead to differences in the observed luminosity distributions of the two types of CEMP stars.

5.4. Other Elements

Figure 12 shows the abundance ratios ($[X/Fe]$) as functions of $[Fe/H]$ for elements other than C, N, and Ba. The abundances of non-CEMP stars are adopted from Cayrel et al. (2004), Honda et al.

⁹This is not the case for non-CEMP stars, for which no selection from the G-band is made in the sample selection.

(2004b), and Aoki et al. (2005). Besides these sources, the results of Gratton et al. (2000) are also shown for Na abundances, while those of Stephens & Boesgaard (2002) are shown for Na, Mg, Ca, Ti, Cr, and Ni abundances. The distributions of the abundance ratios of Sc, Ti, Cr, Ni, and Zn in CEMP stars are quite similar to those in non carbon-enhanced stars. A few stars appear to deviate from the observed trends. For instance, HE 1319–1935 ($[\text{Fe}/\text{H}] = -1.8$) has $[\text{Cr}/\text{Fe}] = +0.75$, and CS 30338–089 has $[\text{Sc}/\text{Fe}] = 1.26$ ($[\text{Fe}/\text{H}] = -2.45$) (both stars are Ba-enhanced objects). However, these results are based on measurements for only one line, and no clear interpretations for these stars can be made at present.

Several CEMP stars exhibit quite high Ca abundances compared to the typical value of non-CEMP stars ($[\text{Ca}/\text{Fe}] \sim +0.3$). In our sample, three stars (HE 1429–0551, HE 1528–0409, and HE 2221–0453) have $[\text{Ca}/\text{Fe}] > +0.8$. However, the abundances are determined from only 1–3 Ca I lines in 5500–6200 Å. The three objects are relatively cool and exhibit large carbon excesses; numerous C_2 and CN molecular lines exist in this wavelength range. Hence, the Ca abundances of such objects are possibly overestimated due to contamination by molecular features. Five stars from the literature have $[\text{Ca}/\text{Fe}] > +0.8$ (Table 14). One is CS 31062–050, studied by Aoki et al. (2002c), who measured the abundance from two Ca I lines in the blue range. However, these lines are possibly affected by CH molecular lines. Indeed, an analysis for 15 Ca I lines in the red spectrum of CS 31062–050, which is used for the analysis of Na lines in the present work, results in $[\text{Ca}/\text{Fe}] = +0.40$ (contamination by C_2 and CN molecular lines is not severe in the red spectrum of this object). We conclude that our previous measurement overestimated the Ca abundance for this object. The other four objects having $[\text{Ca}/\text{Fe}] > +0.8$ were studied by Cohen et al. (2006), who measured the Ca abundances for blue lines as Aoki et al. (2002c) did. The four stars are cool giants having large excesses of carbon. Although we cannot further investigate the Ca abundances of these stars, because red spectra for them are not available, our re-analysis for CS 31062–050 suggests that the analyses for blue lines in CEMP stars possibly overestimate the Ca abundances. Hence, we here do not regard the large Ca overabundances found in several objects as general characteristics of CEMP stars.

In contrast, a large range of abundance ratios is found for Na and Mg. We find moderate overabundances of Mg for most of the CEMP stars in our sample, as is usually observed for non carbon-enhanced stars, but three stars in our sample exhibit large excesses of Mg. One such star is HE 1447+0102 ($[\text{Fe}/\text{H}] = -2.5$), whose Mg abundance ($[\text{Mg}/\text{Fe}] = +1.43$) is determined from the Mg I 5172 Å line alone, with a correspondingly large uncertainty. The Mg abundances of CS 29497–034 ($[\text{Mg}/\text{Fe}] = +1.31$, $[\text{Fe}/\text{H}] = -2.91$) and CS 29528–028 ($[\text{Mg}/\text{Fe}] = +1.69$, $[\text{Fe}/\text{H}] = -2.86$) are, however, based on measurements for three lines, and the scatter of abundances derived from individual lines is not significantly large. Therefore, we suggest that these two stars have distinguishable excesses of Mg from other metal-poor stars. It should be noted that Hill et al. (2000) and Barbuy et al. (2005) reported an excess of this element in CS 29497–034, although the Mg abundance derived by their work is not as high as our present result (see § 3.5). Other stars with excesses of Mg studied by previous work are LP 625–44 ($[\text{Fe}/\text{H}] = -2.7$; Aoki et al. 2002a),

CS 22949–037 ($[\text{Fe}/\text{H}] = -4.0$; e.g., Depagne et al. 2002), and CS 29498–043 ($[\text{Fe}/\text{H}] = -3.5$; e.g., Aoki et al. 2004). The origin of the Mg excesses in the latter two stars has been suggested to be “faint supernovae” explosions that ejected only a small amount of material surrounding the iron core (Tsujimoto & Shigeyama 2003; Umeda & Nomoto 2003). On the other hand, the sources of Mg in other Mg-enhanced CEMP stars are still unknown. We note that LP 625–44, CS 22949–037, and CS 29498–043 also exhibit large overabundances of oxygen (see references above). For the two stars with Mg excesses in our sample, no useful constraint on the oxygen abundance has been obtained at present. Measurements of oxygen abundances for these stars, possibly from the triplet lines at 7770 Å or near-infrared CO lines, are strongly recommended.

The Na abundances of CEMP stars exhibit a large range of enhancements. Although some uncertainties arising from non-LTE corrections and the treatment of damping exist in the determinations of Na abundances, this large scatter cannot be fully explained by measurement errors alone. Previous evidence (Pilachowski et al. 1996; Gratton et al. 2000) points to there being a slight increase in $[\text{Na}/\text{Fe}]$ in more evolved, metal-poor red giants. The former work suggests values around $[\text{Na}/\text{Fe}] = -0.25$ for field subgiants, $[\text{Na}/\text{Fe}] = -0.17$ for field giants, and possibly higher values in globular-cluster giants. Many Ba-enhanced CEMP stars deviate in their sodium abundances from the solar ratios. In order to investigate the correlation between the excesses of carbon and Na, we show $[\text{Na}/\text{Fe}]$ as a function of $[(\text{C}+\text{N})/\text{Fe}]$ in Figure 13. In this Figure, Ba-enhanced and Ba-normal CEMP stars are shown by filled and open symbols, respectively. A clear correlation is found for the 14 Ba-enhanced stars in our sample (filled circles) for which C, N, and Na abundances are determined (as confirmed by the rank correlation test at the 99% confidence level), while the correlation is weaker for the full sample of Ba-enhanced objects. We can at least conclude that Na-enhanced stars also have high $[(\text{C}+\text{N})/\text{Fe}]$ values. The Mg-enhanced stars CS 29497–034 and CS 29528–028 exhibit very large enhancements of Na ($[\text{Na}/\text{Fe}] = +2.74$ and $+1.78$, respectively). The iron abundances of these two stars are very low ($[\text{Fe}/\text{H}] \sim -2.9$) while their excesses of C, N, and Ba are very high, as compared to the rest of our sample. These two stars can be regarded as extreme cases of the Ba-enhanced CEMP stars.

Sodium abundances have also been determined for seven Ba-normal CEMP stars in the present sample (in addition to these stars, HE 0107–5240 and HE 1327–2326, the objects having $[\text{Fe}/\text{H}] < -5$, and the dwarf carbon star G77–61, are also shown by open triangles in the Figure). Four stars among them do not deviate significantly from solar ratios, or have lower values. The carbon excess in these stars is moderate ($[\text{C}/\text{Fe}] \sim +1.0$). This class of objects was first reported by Aoki et al. (2002b), and possibly is a separate class from the other three Ba-normal, extremely carbon-enhanced objects. The two Ba-normal α -element-enhanced CEMP stars, CS 22949–037 and CS 29498–043, both have large enhancements of Na. The other extremely carbon-rich CEMP star, CS 22957–027, also exhibits a large excess of Na. Although the abundances of α -elements in CS 22957–027 are normal, this star could be related in some manner to the above two α -element-enhanced objects.

5.5. Origins of Carbon Excess in CEMP stars

As described in § 1, the fraction of carbon-enhanced objects is significant at low metallicity, although the estimate of this fraction is dependent on the definition of carbon-enhanced stars and the methods used to identify them. For instance, Cohen et al. (2005) have claimed that the fraction of CEMP stars in a sample of giants with $[\text{Fe}/\text{H}] < -2.0$ is $14.5 \pm 4\%$. Lucatello et al. (2006), based on high-resolution analyses of a much larger sample of stars, including many earlier-type stars than the Cohen et al. sample, conclude that this fraction is at least $20 \pm 2\%$. An important question is what is (are) the origin(s) of the carbon-enhancement in such objects.

Our results indicate that the majority of CEMP stars are Ba-enhanced objects – the fraction of Ba-enhanced objects is more than 80% in our sample. This trend is particularly remarkable for stars with relatively high metallicity, above $[\text{Fe}/\text{H}] = -2.6$. Therefore, our conclusion is that the large fraction of CEMP stars at low metallicity can be principally attributed to the high efficiency of AGB nucleosynthesis followed by the mass transfer to a surviving companion (Komiya et al. 2006).

At the lowest metallicities, the contribution of Ba-normal stars to the population of CEMP stars becomes large. This is another factor that leads to the increased fraction of carbon-enhanced stars at low metallicity. The most extreme cases are the carbon-enhanced hyper metal-poor stars with $[\text{Fe}/\text{H}] < -5$ HE 1327–2326 (Frebel et al. 2005) and HE 0107–5240 (Christlieb et al. 2002), for which only upper limits of Ba are determined.

Given the wide distribution of carbon abundances among CEMP stars, as well as the unique abundance patterns of several stars in this class, the CEMP population of stars almost certainly comprises several astrophysical origins. No well-established model exists to explain the Ba-normal CEMP stars, although Ryan et al. (2005) suggested that they form from carbon-rich gas (from a massive progenitor-star population) in contrast to the AGB progenitor paradigm, which explains many features of Ba-enhanced objects.

For the two stars CS 22949–037 and CS 29498–043, large excesses of the α -elements and oxygen are also found, suggesting the contribution of “faint supernova” nucleosynthesis, with the progenitor stars undergoing mixing and fallback (Tsujimoto & Shigeyama 2003; Umeda & Nomoto 2003). A similar interpretation might be applicable to the hyper metal-poor stars with $[\text{Fe}/\text{H}] < -5.0$ (see also Iwamoto et al. 2005), although several other models have been proposed for these stars. One idea is that such stars might have formed from gas polluted by mass loss from early-generation massive, rapidly-rotating stars with $[\text{Fe}/\text{H}] < -6.0$ (Hirschi et al. 2006; Meynet et al. 2006). This model has the additional advantage of being able to account for the otherwise mysterious lack of detected Li in the turnoff star HE 1327–2326 (Hirschi 2006). Piau et al. (2006) have argued that this same population might even be responsible for the alteration of primordial Li from (higher) Big Bang Nucleosynthesis values down to a level consistent with the Spite Plateau Li abundance found in metal-poor turnoff stars. If a significant population of such primordial objects did indeed exist, one might argue that they could be closely related to the astrophysical origin of the Ba-normal

CEMP stars found at quite low metallicity. Karlsson (2006) has appealed to the same progenitors to account for the possible gap in the metallicity distribution of halo stars between $[\text{Fe}/\text{H}] \sim -4.0$ and ~ -5.0 revealed by the HK and HES prism surveys. Also of interest is the recent paper by Chiappini et al. (2006), where their new chemical evolution models *require* the large yields of carbon and nitrogen from the models discussed by Hirschi et al. (2006) in order to account for the upturn of the observed $[\text{N}/\text{O}]$ and $[\text{C}/\text{O}]$ ratios in the “unmixed” carbon-*normal* stars described by Spite et al. (2005).

Other possibilities for the origin of Ba-normal CEMP stars, in particular for the objects having normal abundance ratios of the α -elements, exist. Cohen et al. (2006) suggested that one possible interpretation could be that the s-process in AGB stars with such low metallicities did not produce any distinctive excess of barium. Komiya et al. (2006) have recently proposed that the Ba-normal CEMP stars are the result of nucleosynthesis in extremely metal-poor AGB stars with masses higher than $3.5 M_{\odot}$. Their models of AGB stars, originally developed by Fujimoto et al. (2000), suggest that the s-process does not occur in extremely metal-poor AGB stars in this mass range because of the low efficiency of radiative ^{13}C burning (the case IV’ in their classification). Interestingly, according to their models, this class of AGB stars should have metallicities of $[\text{Fe}/\text{H}] < -2.5$, which is very similar to the metallicity range over which Ba-normal CEMP stars are found (§5.1). Unfortunately, there is no evidence of binarity for most objects in this class. However, according to their models, binary systems having very long orbital periods are able to produce carbon-enhancement by stellar winds from a primary AGB star at very low metallicity. For such long-period binary systems, the present absence of variations in radial velocity is not conclusive. A statistical analysis (e.g., Lucatello et al. 2005) based on large samples of Ba-normal CEMP stars observed over very long temporal baselines will be required in order to test such models.

6. Concluding Remarks

In this paper we have determined chemical abundances for 26 metal-poor stars, and classified 22 stars among them as Carbon-Enhanced Metal-Poor (CEMP) stars, based on a new definition for the carbon-enhancement phenomenon including the effects of evolution along the giant branch on observed carbon abundances. Sodium abundances were determined for another nine CEMP stars for which abundances of other elements were previously studied. Combining the results of previous work for 42 CEMP stars and the 22 other CEMP stars in our present sample, we investigated the abundance trends found in CEMP stars and discussed the origins of carbon excesses in these objects. We found that most CEMP stars (more than 80%) exhibit excesses of neutron-capture elements (e.g., Ba), suggesting significant contributions of AGB nucleosynthesis. However, the fraction of Ba-normal stars increases at lower metallicity. The difference in the metallicity distribution of Ba-enhanced and Ba-normal CEMP stars found in the present work should be a key to understanding the processes responsible for the Ba-normal CEMP stars.

Another difference between the Ba-enhanced and Ba-normal stars is found in their carbon

abundance distributions. While the Ba-enhanced stars have quite high carbon abundances ($-1 \lesssim [\text{C}/\text{H}] \lesssim 0$), independent of their metallicity, the $[\text{C}/\text{H}]$ values of Ba-normal CEMP stars distribute over a wide range, while their average value is relatively low. This difference also suggests that the processes responsible for the Ba-normal CEMP stars are quite different from the AGB nucleosynthesis that can explain the chemical abundances of Ba-enhanced CEMP stars.

Some possible interpretations are proposed for the origin of Ba-normal CEMP stars, in particular for the α -element-enhanced stars. Moreover, these stars are likely to be closely related to the two known hyper metal-poor stars with $[\text{Fe}/\text{H}]$ below -5 . However, the sample of such stars studied with high-resolution spectroscopy is still quite small (ten objects in the present sample). Further observations for this class of objects are strongly recommended.

Measurements of abundances for Ba-enhanced CEMP stars based on high-resolution spectroscopy have been rapidly increasing in recent years. Although the abundances of these objects are usually interpreted within the paradigm of AGB nucleosynthesis and mass transfer in binary systems, their detailed abundance patterns are not well explained by current models. One example is the abundance pattern found for objects with very large excesses of neutron-capture elements, which cannot be explained by the present AGB models. Several CEMP stars are known to have enhancements of both r- and s-process elements, the so-called CEMP-r/s stars. More detailed abundance studies, as well as the monitoring of radial velocities to investigate their binarity, are strongly desired. We plan to investigate these problems in future papers in this series.

W.A. is grateful for useful discussions on the nucleosynthesis and evolution of CEMP stars with Drs. M. Y. Fujimoto and T. Suda. J.E.N. acknowledges support from Australian Research Council grant DP0342613. T.C.B. acknowledges partial support from a series of grants awarded by the US National Science Foundation, most recently, AST 04-06784, as well as from grant PHY 02-16783; Physics Frontier Center/Joint Institute for Nuclear Astrophysics (JINA). N.C. acknowledges support from Deutsche Forschungsgemeinschaft under grants Ch 214/3 and Re 353/44.

A. CEMP Stars Investigated in the Present Work

In this paper we discussed the abundances and evolutionary status for 22 CEMP stars analyzed by the present work and 42 CEMP stars that have been previously studied. Table 14 lists the abundances and atmospheric parameters of CEMP stars discussed in § 4 and § 5. References are provided in the last column of the Table. The chemical compositions of the following objects were reported by more than one paper. Here we provide a few comments for these objects and justify our adopted results.

- **CS 22948–027 and CS 29497–034:** These objects were studied in considerable detail by Hill et al. (2000) and Barbuy et al. (2005). Comparisons of their measurements and ours

are discussed in § 3.5. Preston & Sneden (2001) studied binarity, as well as abundances, for CS 22948–027. In the discussion we adopted the results from the present work.

- **CS 22957–027:** Norris et al. (1997b) and Bonifacio et al. (1998) reported abundances for this star. Preston & Sneden (2001) studied its binarity, as well as its elemental abundances. We adopted the results of our previous work (Aoki et al. 2002c,d), based on spectra of higher quality than previously available. The Na abundance of this object was determined by the present work. Preston & Sneden (2001) also reported a large excess of Na, although their value of $[\text{Na}/\text{Fe}]$ is 0.5 dex lower than ours. We note that our result is based on abundances from subordinate lines and the non-LTE corrected abundances from D lines (see §3.3).
- **CS 22898–027:** McWilliam et al. (1995) reported the abundances of this object for the first time. Its binarity and abundances were studied by Preston & Sneden (2001). We adopted the results of our previous work (Aoki et al. 2002c,d), based on spectra with remarkably higher quality than available previously. The Na abundance was determined in the present work.
- **CS 22942–019:** We adopted the results of our previous studies (Aoki et al. 2002c,d). This star was also analyzed by Preston & Sneden (2001), who derived results similar to ours. We adopted their Na abundance.
- **CS 31062–050:** The abundances determined by our previous work (Aoki et al. 2002c,d) were adopted. This object was also studied by Johnson & Bolte (2004), based on high quality spectra. Their results for elements discussed in the present paper agree within the errors with our previous work. An exception is the Ba abundance ratio, for which Johnson & Bolte (2004) derived a value 0.5 dex higher than ours.
- **CS 22880–074:** The results of our previous studies (Aoki et al. 2002c,d) and the present work for the Na abundance were adopted. This object was also studied by Preston & Sneden (2001). The abundances derived by them agree within 0.3 dex with our results. An exception is the Mg abundance, for which Preston & Sneden (2001) derived a quite low value ($[\text{Mg}/\text{Fe}] = 0.06$) compared to other metal-poor stars.
- **CS 29502–092:** The abundances determined by Aoki et al. (2002a) were adopted. This object was more recently studied by Tsangarides (2005), who compared in some detail their results with those of Aoki et al. (2002a).
- **CS 29497–030:** This object was studied by Sneden et al. (2003) and Sivarani et al. (2004). More recently, Ivans et al. (2005) made a more comprehensive abundance analysis using higher quality spectra. We adopted the results of Ivans et al. (2005).
- **CS 22949–037:** The abundances of this object were reported by McWilliam et al. (1995) for the first time. This object was re-investigated by Norris et al. (2001, 2002), Depagne et al. (2002), and Cayrel et al. (2004). We adopted the results by Depagne et al. (2002), who

made the most comprehensive abundance analysis. An exception is the Na abundance, for which we adopted the result of Cayrel et al. (2004), who corrected the value of Depagne et al. (2002) using the same spectra.

- **CS 22183–015:** This object was studied by Johnson & Bolte (2002), in particular for the neutron-capture elements. Abundances of this object, including those of light elements not measured by Johnson & Bolte (2002), were recently reported by Cohen et al. (2006). Here we adopted the results by Cohen et al. (2006).

REFERENCES

- Alonso, A., Arribas, S., & Martínez-Roger, C. 1996, *A&A*, 313, 873
- Alonso, A., Arribas, S., & Martínez-Roger, C. 1999, *A&AS*, 140, 261
- Aoki, W., & Tsuji, T. 1997, *A&A*, 317, 845
- Aoki, W. et al. 2002a, *PASJ*, 54, 427
- Aoki, W., Norris, J. E., Ryan, S. G., Beers, T. C., & Ando, H. 2002b, *ApJ*, 567, 1166
- Aoki, W., Norris, J. E., Ryan, S. G., Beers, T. C., & Ando, H. 2002c, *PASJ*, 54, 933
- Aoki, W., Ryan, S. G., Norris, J. E., Beers, T. C., Ando, H., & Tsangarides, S. 2002d, *ApJ*, 580, 1149
- Aoki, W., Norris, J. E., Ryan, S. G., Beers, T. C., Christlieb, N., Tsangarides, S., & Ando, H. 2004, *ApJ*, 608, 971
- Aoki, W., et al. 2005, *ApJ*, 632, 611
- Arlandini, C., Käppeler, F., Wisshak, K., Gallino, R., Lugaro, M., Busso, M. & Straniero, O. 1999, *ApJ*, 525, 886
- Asplund, M. 2005, *ARA&A*, 43, 481
- Asplund, M., Grevesse, N., Sauval, A. J., Allende Prieto, C., & Blomme, R. 2005, *A&A*, 431, 693
- Barbuy, B., Cayrel, R., Spite, M., Beers, T.C., Spite, F., Nordström, B., & Nissen, P. E. 1997, *A&A*, 317, L63
- Barbuy, B., Spite, M., Spite, F., Hill, V., Cayrel, R., Plez, B., & Petitjean, P. 2005, *A&A*, 429, 1031
- Barklem, P. S., et al. 2005, *A&A*, 439, 129

- Beers, T.C. 1999, in Third Stromlo Symposium: The Galactic Halo, eds. Gibson, B.K., Axelrod, T.S. & Putman, M.E., ASP Conference Series Vol. 165, p. 206
- Beers, T. C., & Christlieb, N. 2005, *ARA&A*, 43, 531
- Beers, T. C., Preston, G. W., & Shectman, S. A. 1992, *AJ*, 103, 1987
- Beers, T. C., et al. 2006, *ApJS*, submitted
- Bond, H. E. 1974, *ApJ*, 194, 95
- Bonifacio, P., Molaro, P., Beers, T.C., & Vladilo, G. 1998, *A&A*, 332, 672
- Cayrel, R., et al. 2004, *A&A*, 416, 1117
- Charbonnel, C. 1995, *ApJ*, 453, L41
- Chiappini, C., Hirschi, R., Meynet, G., Ekström, S., Maeder, A., & Matteucci, F. 2006, *A&A*, 449, 27
- Christlieb, N. 2003, *Reviews in Modern Astronomy*, Vol. 16, ed. R. Schielicke (Wiley-VCH, Berlin), 191
- Christlieb, N., et al. 2002, *Nature*, 419, 904
- Christlieb, N., Green, P. J., Wisotzki, L., & Reimers, D. 2001, *A&A*, 375, 366
- Cohen, J. G., Christlieb, N., Qian, Y. -Z, & Wasserburg, G. J. 2003, *ApJ*, 588, 1082
- Cohen, J. G., et al. 2004, *ApJ*, 612, 1107
- Cohen, J. G., et al. 2005, *ApJ*, 633, L109
- Cohen, J. G., et al. 2006, *AJ*, 132, 137
- Depagne, E. et al. 2002, *A&A*, 390, 187
- Frebel, A., et al. 2005, *Nature*, 434, 871
- Fujimoto, M. Y., Ikeda, Y., & Iben, I. Jr 2000, *ApJ*, 529, L25
- Goswami, A., Aoki, W., Beers, T. C., Christlieb, N., Norris, J. E., Ryan, S. G. 2006, *MNRAS*, in press
- Gratton, R. G., Carretta, E., Eriksson, K., & Gustafsson, B. 1999, *A&A*, 350, 955
- Gratton, R. G., Sneden, C., Carretta, E., & Bragaglia, A. 2000, *A&A*, 354, 169
- Green, P. J., Margon, B., Anderson, S. F., & Cook, K. H. 1994, *ApJ*, 434, 319

- Hill, V., et al. 2000, *A&A*, 353, 557
- Hirschi, R. 2006, in Proceedings of “Origins of Matter and Evolution of Galaxies (OMEG05): New Horizons of Nuclear Astrophysics and Cosmology,” (ed. S. Kubono, W. Aoki, T. Kajino, T. Motobayashi, K. Nomoto), AIP Conf. Proc. 847, 71 (astro-ph/0601498)
- Hirschi, R., Fröhlich, C., Liebendorfer, M., & Thielemann, F.-K. 2006, in *Reviews of Modern Astronomy* 19, in press (astro-ph/0601502)
- Honda, S. et al. 2004a, *ApJS*, 152, 113
- Honda, S., Aoki, W., Kajino, T., Ando, H., Beers, T. C., Izumiura, H., Sadakane, K., & Takada-Hidai, M. 2004b, *ApJ*, 607, 474
- Ivans, I. I., Sneden, C., Gallino, R., Cowan, J. J., & Preston, G. W. 2005, *ApJ*, 627, L145
- Iwamoto, N., Umeda, H., Tominaga, N., Nomoto, K., & Maeda, K. 2005, *Science*, 309, 451
- Johnson, J. A., & Bolte, M. 2002, *ApJ*, 579, L87
- Johnson, J. A., & Bolte, M. 2004, *ApJ*, 605, 462
- Jonsell, K., Barklem, P. S., Gustafsson, B., Christlieb, N., Hill, V., Beers, T. C., & Holmberg, J. 2006, *A&A* 451, 651
- Karlsson, T. 2006, *ApJ*, 641, L41
- Keenan, P. C., *ApJ*, 96, 101
- Komiya, Y., Suda, T., Minaguchi, H., Shigeyama, T., Aoki, W., & M. Y. Fujimoto 2006, *ApJ*, submitted
- Kurucz, R. L., 1993, CD-ROM 13, *ATLAS9 Stellar Atmospheres Programs and 2 km/s Grid* (Cambridge: Smithsonian Astrophys. Obs.)
- Lawler, J. E., Bonvallet, G., & Sneden, C. 2001, *ApJ*, 556, 452
- Lucatello, S., Gratton, R., Cohen, J. G., Beers, T. C., Christlieb, N., Carretta, E., & Ramírez, S. 2003, *AJ*, 125, 875
- Lucatello, S., Tsangarides, S., Beers, T. C., Christlieb, N., Carretta, E., Gratton, R. G. & Ryan, S. G. 2005, *ApJ*, 625, 825
- Lucatello, S., Beers, T.C., Christlieb, N., Barklem, P.S., Rossi, S., Marsteller, B., Sivarani, T., & Lee, Y., *ApJ*, submitted
- Magain, P. 1988, *IAU Symp.* 132: The Impact of Very High S/N Spectroscopy on Stellar Physics, 132, 485

- Masseron, T., Van Eck, S., Famaey, B., Goreily, S., Plez, B., Siess, L., Beers, T.C., Primas, F., & Jorissen, A. 2006, A&A, in press (astro-ph/0605658)
- McClure, R. D. 1984, ApJ, 280, L31
- McClure, R. D. & Woodsworth, A. W. 1990, ApJ, 352, 709
- McWilliam, A. 1998, AJ, 115, 1640
- McWilliam, A., Preston, G. W., Sneden, C., & Searle, L. 1995, AJ, 109, 2757
- Meynet, G., Ekström, S., & Maeder, A. 2006, A&A, 447, 623
- Noguchi, K., Aoki, W., Kawanomoto, S., et al. 2002, PASJ, 54, 855
- Norris, J. E., Ryan, S. G., & Beers, T. C. 1997a, ApJ, 488, 350
- Norris, J. E., Ryan, S. G., & Beers, T. C. 1997b, ApJ, 489, L169
- Norris, J. E., Ryan, S. G., & Beers, T. C. 2001, ApJ, 561, 1034
- Norris, J. E., Ryan, S. G., Beers, T. C., Aoki, W., & Ando, H. 2002, ApJ, 569, L107
- Piau, L., Beers, T.C., Balsara, D.S., Sivarani, T., Truran, J.W., & Ferguson, J.W. 2006, ApJ, submitted (astro-ph/0603553)
- Pilachowski, C. A., Sneden, C., & Kraft, R. P. 1996, AJ, 111, 1689
- Plez, B., & Cohen, J. G. 2005, A&A, 434, 1117
- Preston, G. W. & Sneden, C. 2001, AJ, 122, 1545
- Ryan S. G., Aoki W., Norris J.E., Beers T.C. 2005, ApJ, 635, 349
- Ryan, S. G., Norris, J. E., & Beers, T. C. 1996, ApJ, 471, 254
- Schlegel, D.J., Finkbeiner, D.P., & Davis, M. 1998, ApJ, 500, 525
- Sivarani, T., et al. 2004, A&A, 413, 1073
- Skrutskie, M. F., et al. 2006, AJ, 131, 1163
- Sneden, C., Preston, G. W., & Cowan, J. J. 2003, ApJ, 592, 504
- Sneden, C., McWilliam, A., Preston, G. W., Cowan, J. J., Burris, D. L., & Armosky, B. J. 1996, ApJ, 467, 819
- Spite, M., Cayrel, R., Plez, B., Hill, V., Spite, F., Depagne, E., Francois, P., Bonifacio, P., Barbuy, B., Beers, T.C., Andersen, J., Molaro, P., Nordström, B., & Primas, F. 2005, A&A, 430, 655

- Stephens, A., & Boesgaard, A. M. 2002, *AJ*, 123, 1647
- Takeda, Y., Zhao, G., Takada-Hidai, M., Chen, Y.-Q., Saito, Y.-J., & Zhang, H.-W. 2003, *Chinese Journal of Astronomy and Astrophysics*, 3, 316
- Thévenin, F., & Idiart, T. P. 1999, *ApJ*, 521, 753
- Totten, E.J., & Irwin, M.J. 1998, *MNRAS*, 294, 1
- Totten, E.J., Irwin, M.J., & Whitelock, P.A. 2000, *MNRAS*, 314, 630
- Tsangarides, S. A. 2005, PhD theses (The Open University)
- Tsujimoto, T., & Shigeyama, T. 2003, *ApJ*, 584, L87
- Umeda, H., & Nomoto, K. 2003, *Nature*, 422, 871
- van den Hoek, L. B., & Groenewegen, M. A. T. 1997, *A&AS*, 123, 305
- Vanture, A. D. 1992, *AJ*, 104, 1997
- Ventura, P., D’Antona, F., & Mazzitelli, I. 2002, *A&A*, 393, 215
- Wallerstein, G., & Greenstein, J. L. 1963, *AJ*, 68, 546

Table 1. OBJECT LIST AND OBSERVING LOG

ID	Object	RA(2000)	Dec(2000)	Exp. Time (sec)	Count (5200 Å)	Obs.date (UT)	V_r km s ⁻¹	s.e. ^a km s ⁻¹
1	BS 16929–005	13:03:29.4	+33:51:06	600	1800	May 25, 2003	–50.4	0.13
2	CS 22174–007	01:14:06.7	–11:02:32	600	6700	Oct 26, 2002	–70.76	0.03
3	CS 22886–042	22:20:25.9	–10:23:20	600	2300	Oct 26, 2002	–221.4	0.05
4	CS 22948–027	21:37:45.4	–39:27:20	600	3100	Oct 26, 2002	–62.49	0.09
5	CS 22960–053	22:16:17.0	–43:54:21	2400	1900	Oct 26, 2002	282.26	0.08
6	CS 29503–010	00:04:55.4	–24:24:19	900	2500	Oct 26, 2002	–24.28	0.04
7	CS 29528–028	02:28:26.5	–21:33:00	1200	1500	Oct 26, 2002
	CS 29528–028	3000	3000	Oct 28, 2002	58.23	0.34
8	CS 30312–100	15:43:31.8	+02:01:18	150	1000	May 25, 2003	–122.66	0.12
9	CS 30322–023	21:30:32.0	–46:16:31	600	3200	Oct 26, 2002	116.47	0.07
10	CS 30338–089	23:15:50.1	+10:19:26	900	2000	Oct 26, 2002	–113.06	0.10
11	CS 31062–041	00:35:02.9	–15:54:36	1200	2500	Oct 26, 2002	–172.45	0.05
12	CS 29497–034 ^b	00:41:39.7	–26:18:53	1200	7000	Oct 26, 2002	–49.52	0.10
13	HE 0206–1916	02:09:19.6	–19:01:56	1200	2200	Oct 26, 2002	–200.01	0.09
14	HE 0400–2030	04:02:14.8	–20:21:53	900	1900	Oct 26, 2002	221.83	0.05
15	HE 0441–0652	04:43:29.8	–06:46:54	1800	3000	Oct 26, 2002	–29.77	0.05
16	HE 0507–1653	05:09:16.5	–16:50:05	1200	10500	Oct 26, 2002	353.01	0.07
17	HE 1005–1439	10:07:52.3	–14:54:20	1800	1250	Oct 26, 2002	86.87	0.20
18	HE 1157–0518	12:00:18.1	–05:34:43	1800	1050	May 25, 2003	142.91	0.26
19	HE 1319–1935	13 22 38.7	–19 51 11	900	1000	May 25, 2003	368.98	0.11
20	HE 1429–0551	14:32:31.3	–06:05:00	600	2600	May 25, 2003	–44.94	0.11
21	HE 1447+0102	14:50:15.1	+00:50:15	1500	1800	May 25, 2003	–61.22	0.21
22	HE 1523–1155	15:26:41.0	–12:05:43	600	3500	May 26, 2003	–45.03	0.12
23	HE 1528–0409	15 30 54.3	–04 19 40	1500	1300	May 25, 2003	–157.48	0.25
24	HE 2221–0453	22:24:25.7	–04:38:02	900	3000	Oct 26, 2002	–189.91	0.13
25	HE 2228–0706	22:31:24.5	–06:50:51	900	4000	Oct 26, 2002	–11.69	0.12
26	HE 2330–0555	23:32:54.8	–05:38:50	1200	1500	Oct 26, 2002	–235.03	0.09

^aStandard error of radial velocity σ/\sqrt{n} , where σ is the standard deviation of the values from individual lines and n is the number of lines used.

^bCS 29497–034 = HE 0039–2635

Table 2. PHOTOMETRIC DATA

ID	Object	B	V	R	I	J	H	K	$E(B - V)$	$T_{\text{eff}}(V - K)$	$\Delta T_{\text{eff}}^{\text{a}}$
1	BS 16929-005	14.228	13.610	13.208	12.766	12.170	11.750	11.670	0.01	5257	31
2	CS 22174-007	13.103	12.409	11.961	11.509	10.885	10.404	10.318	0.08	5309	-21
3	CS 22886-042	14.106	13.275	12.763	12.269	11.511	11.028	10.940	0.03	4830	-36
4	CS 22948-027	13.790	12.660	12.160	11.760	10.979	10.534	10.427	0.08	5135	-298
5	CS 22960-053	15.705	14.950	14.537	14.046	13.298	12.833	12.761	0.07	5160	-121
6	CS 29503-010	14.209	13.737	13.430	13.128	12.726	12.468	12.433	0.08	6532	-33
7	CS 29528-028	14.862	14.510	14.292	14.015	13.755	13.535	13.537	0.03	7046	248
8	CS 30312-100	13.629	12.916	12.444	11.995	11.390	10.946	10.879	0.05	5256	105
9	CS 30332-023	13.460	12.200	11.498	10.908	10.050	9.479	9.313	0.03	4344	2
10	CS 30338-089	15.107	14.144	13.632	13.176	12.558	12.046	12.000	0.01	4985	72
11	CS 31062-041	14.754	13.934	13.476	12.984	12.389	11.926	11.821	0.03	5066	104
12	CS 29497-034	13.338	12.221	11.704	11.321	10.571	10.115	9.996	0.05	5037	-340
13	HE 0206-1916	15.133	13.999	13.458	12.987	12.243	11.765	11.660	0.13	5161	-76
14	HE 0400-2030	14.921	14.033	13.605	13.164	12.494	12.064	11.975	0.13	5519	-74
15	HE 0441-0652	15.250	14.228	13.678	13.106	12.354	11.828	11.706	0.11	4864	44
16	HE 0507-1653	13.633	12.507	12.002	11.579	10.883	10.430	10.315	0.03	4980	-71
17	HE 1005-1439	14.440	13.524	13.054	12.515	12.240	11.754	11.696	0.03	5512	651
18	HE 1157-0518	16.273	15.120	14.635	14.128	13.418	12.917	12.846	0.03	4875	13
19	HE 1319-1935	15.698	14.198	13.630	13.167	12.334	11.769	11.681	0.03	4635	-175
20	HE 1429-0551	14.015	12.606	11.995	11.537	10.734	10.272	10.066	0.05	4681	-191
21	HE 1447+0102	15.632	14.614	14.121	13.676	13.207	12.760	12.682	0.02	5285	274
22	HE 1523-1155	14.571	13.225	12.622	12.138	11.372	10.846	10.748	0.05	4750	-56
23	HE 1528-0409	16.003	14.757	14.159	13.681	12.945	12.455	12.358	0.10	4994	-7
24	HE 2221-0453	15.098	13.650	12.942	12.376	11.524	10.997	10.815	0.04	4378	15
25	HE 2228-0706	14.353	13.332	12.797	12.353	11.692	11.289	11.192	0.05	5130	87
26	HE 2330-0555	15.412	14.559	14.158	13.612	12.850	12.395	12.300	0.03	4915	-74

^a $\Delta(T_{\text{eff}}) = T_{\text{eff}}(V - K)_{\text{0}} - < T_{\text{eff}}(V - R)_{\text{0}}, T_{\text{eff}}(V - I)_{\text{0}}, T_{\text{eff}}(R - I)_{\text{0}} >$

Table 3. OBJECT LIST AND OBSERVING LOG

ID	Object (sec)	Exp. Time (5900 Å)	Count	Obs.date (UT)
Na1	HD 196944	30	17500	Sep 13, 2005
Na2	LP 706–7	180	2500	Sep 18, 2005
Na3	CS 22183–015 ^a	600	2200	June 17, 2005
Na4	CS 22880–074	3000	5500	June 18, 2005
Na5	CS 22898–027	3000	15000	July 3, 2000
Na6	CS 22957–027	5330	17800	June 18, 2005
Na7	CS 29526–110	720	3500	Sep 18, 2005
Na8	CS 30301–015	300	1900	Sep 13, 2005
Na9	CS 31062–050	3600	22200	June 29, 2005

^aCS 22183–015 = HE 0058–0244

Table 4. EQUIVALENT WIDTHS

Species	Wavelength (Å)	L.E.P. (eV)	$\log gf$	W_λ (mÅ)								
				(1)	(2)	(3)	(4)	(5)	(6)	(7)	(8)	(9)
Na I	5688.20	2.10	−0.46	5.3	38.8	...	11.1
Na I	5889.95	0.00	0.10	95.5	161.9	164.8	195.8	...	153.7	194.6	147.8	...
Na I	5895.92	0.00	−0.20	64.2	141.5	137.6	188.5	172.0x	147.2	183.8	126.0	...
Mg I	4571.10	0.00	−5.69	...	54.6	58.1	26.9	...	38.5	99.5
Mg I	4702.99	4.35	−0.52	28.6	67.1	70.5	55.8	63.2	...
Mg I	5172.69	2.71	−0.38	128.5	191.9	174.9	191.1	130.4	...	141.4	180.3	190.5
Mg I	5183.60	2.72	−0.16	143.1	215.5	190.2	...	146.1	...	157.3	202.4	...
Mg I	5528.40	4.35	−0.49	28.0	69.0	66.9	...	41.8	103.6	...	64.7	71.0
Ca I	4226.73	0.00	0.24	124.9	87.7	188.4	...
Ca I	4318.65	1.90	−0.21	38.8	...
Ca I	4425.44	1.88	−0.36	...	53.3	49.4	72.3	...	42.2	...
Ca I	4434.96	1.89	−0.01	89.8
Ca I	4455.89	1.90	−0.53	...	42.7	32.8	59.0	...	32.5	...
Ca I	5265.56	2.52	−0.11	...	27.9	27.5	51.2	16.3
Ca I	5581.97	2.52	−0.56	16.9	29.9
Ca I	5588.76	2.53	0.36	...	49.5	41.8	61.3	...	74.4	...	35.6	24.0
Ca I	5594.47	2.52	0.10	...	40.1	31.5	79.0	...	62.4	...	27.0	25.2
Ca I	5601.29	2.53	−0.52	...	15.2	...	122.5	...	30.5
Ca I	5857.45	2.93	0.24	...	26.7	21.7	64.2	...	46.2	...	25.4	...
Ca I	6102.72	1.88	−0.77	...	34.5	29.9	51.2	...	48.7	...	21.9	...
Ca I	6122.22	1.89	−0.32	...	59.5	54.9	91.4	23.8	75.5	...	47.6	51.7
Ca I	6162.17	1.90	−0.09	22.0	72.1	67.3	...	30.3	83.9	...	67.0	68.8
Ti I	4533.24	0.85	0.53	...	49.3	45.7	42.3	...	40.5	35.0
Ti I	4981.73	0.85	0.56	...	55.6	51.5	46.6	...	45.4	47.0
Ti I	4991.07	0.84	0.44	...	51.0	47.9	58.0	...	44.6	43.8
Ti I	4999.50	0.83	0.31	...	43.8	49.9	49.7	...	35.3	43.3
Ti I	5007.21	0.82	0.17	...	47.5	45.5	61.4	...	47.5	32.2
Ti I	5173.74	0.00	−1.06	...	24.9	17.2	54.8	21.4	24.1
Ti I	5192.97	0.02	−0.95	...	29.6	21.9	68.7	21.2	...
Ti I	5206.08	2.49	1.07	22.9	68.9
Ti I	5210.38	0.05	−0.83	...	34.9	25.2	45.5	31.2	28.2
Cr I	4616.14	0.98	−1.19	...	13.9
Cr I	4626.19	0.97	−1.32	21.1	...
Cr I	4646.17	1.03	−0.70	...	29.5	31.1	37.0	...	39.1	...
Cr I	4651.29	0.98	−1.46	...	9.1
Cr I	4652.16	1.00	−1.03	...	19.7
Cr I	5208.44	0.94	0.16	30.3	88.1	87.7	100.8	38.7	94.6	95.8
Cr I	5298.27	0.98	−1.15	...	18.4
Cr I	5409.79	1.03	−0.72	...	32.6	33.4	67.4	...	41.9	33.5

Table 4—Continued

Species	Wavelength (Å)	L.E.P. (eV)	$\log gf$	W_λ (mÅ)								
				(1)	(2)	(3)	(4)	(5)	(6)	(7)	(8)	(9)
Fe I	4383.54	1.49	0.20	161.4	...
Fe I	4407.71	2.18	−1.97	...	38.5	50.1	43.5
Fe I	4408.41	2.20	−1.77	...	43.6	41.0	44.2
Fe I	4415.12	1.61	−0.62	38.6
Fe I	4422.57	2.85	−1.11	...	36.3	40.2
Fe I	4430.61	2.22	−1.66	8.9	40.8	44.1	42.3	...	35.9	...
Fe I	4433.22	3.65	−0.70	...	16.3
Fe I	4442.34	2.20	−1.25	...	65.9	65.7	74.7	...	56.3	86.5
Fe I	4443.19	2.86	−1.04	...	31.7	27.0	47.6	20.5
Fe I	4447.72	2.22	−1.34	13.0	57.2	67.6	63.5	...	54.6	68.1
Fe I	4461.65	0.09	−3.21	39.0	88.8	97.0	60.6	...	81.5	150.4
Fe I	4466.55	2.83	−0.60	16.2	67.0	63.8	67.2	...	57.9	81.3
Fe I	4476.02	2.85	−0.82	...	52.4	52.8	48.8	...
Fe I	4484.22	3.60	−0.86	...	15.6	18.9
Fe I	4489.74	0.12	−3.97	12.1	54.0	66.6	31.3	...	39.2	106.5
Fe I	4494.56	2.20	−1.14	20.8	67.2	71.7	65.8	...	62.1	...
Fe I	4528.61	2.18	−0.82	33.8	86.3	83.2	80.2	104.7
Fe I	4531.15	1.49	−2.15	14.6	60.2	65.5	57.4	...	55.7	87.1
Fe I	4592.65	1.56	−2.45	...	43.1	51.3	43.3	...	32.8	50.3
Fe I	4602.94	1.49	−2.21	16.3	60.5	71.1	49.4	...	45.0	75.2
Fe I	4733.59	1.49	−2.99	...	22.0	27.0	23.4
Fe I	4736.77	3.21	−0.75	...	35.2	34.4	48.0	...	35.6	...
Fe I	4871.32	2.87	−0.36	28.3	66.2	72.5	...	23.3	77.9	...	59.5	62.7
Fe I	4872.14	2.88	−0.57	14.5	54.0	49.4	68.1	...	48.8	48.6
Fe I	4890.75	2.88	−0.39	18.5	65.6	69.0	...	28.6	87.9	...	65.6	68.8
Fe I	4891.49	2.85	−0.11	33.1	80.9	80.2	...	41.3	93.3	...	74.3	74.8
Fe I	4903.31	2.88	−0.93	...	40.6	46.6	57.8	...	32.9	31.2
Fe I	4918.99	2.87	−0.34	21.3	68.4	67.6	82.6	...	71.2	63.3
Fe I	4920.50	2.83	0.07	39.5	86.9	91.2	...	42.6	...	21.5	86.4	...
Fe I	4924.77	2.28	−2.26	...	19.0	16.8	22.7	21.8
Fe I	4938.81	2.88	−1.08	...	32.7	32.0	49.5	...	38.2	17.7
Fe I	4939.69	0.86	−3.34	...	41.3	51.5	28.8	...	44.9	70.8
Fe I	4994.13	0.92	−2.96	...	52.0	56.3	36.4	...	43.3	79.5
Fe I	5006.12	2.83	−0.61	...	60.6	59.9	72.4	...	52.7	56.4
Fe I	5012.07	0.86	−2.64	27.2	79.0	87.2	...	37.2	59.8	...	69.4	125.2
Fe I	5041.76	1.49	−2.20	...	67.7	69.1	47.8	85.1
Fe I	5049.82	2.28	−1.34	...	54.0	58.5	...	14.9	61.5	...	48.4	57.5
Fe I	5051.63	0.92	−2.80	17.6	68.7	81.1	53.4	...	63.1	105.9
Fe I	5068.77	2.94	−1.04	...	31.2	30.8	45.8	...	35.3	...

Table 4—Continued

Species	Wavelength (Å)	L.E.P. (eV)	$\log gf$	W_λ (mÅ)								
				(1)	(2)	(3)	(4)	(5)	(6)	(7)	(8)	(9)
Fe I	5083.34	0.96	−2.96	...	56.7	59.1	44.5	...	44.0	96.4
Fe I	5110.41	0.00	−3.76	...	77.1	85.3	50.8	144.0
Fe I	5123.72	1.01	−3.07	...	48.5	61.8	47.8	...	31.8	85.3
Fe I	5127.36	0.92	−3.31	...	41.2	46.0	33.1	...	29.6	68.9
Fe I	5133.69	4.18	0.14	...	28.4	21.9	59.6	...	21.0	...
Fe I	5150.84	0.99	−3.00	...	45.9	53.5	30.2	...	37.9	69.1
Fe I	5151.91	1.01	−3.32	...	36.6	37.7	23.5	...	34.1	54.8
Fe I	5162.27	4.18	0.02	...	25.9	17.9	46.3
Fe I	5166.28	0.00	−4.20	...	51.2	67.5	72.8	...	26.4	...	41.1	111.2
Fe I	5171.60	1.49	−1.79	32.5	80.5	91.1	96.1	37.3	72.9	...	74.8	112.0
Fe I	5191.46	3.04	−0.55	...	50.1	53.4	70.5	...	37.0	49.5
Fe I	5192.34	3.00	−0.42	...	59.9	61.3	79.5	...	73.0	...	47.7	49.2
Fe I	5194.94	1.56	−2.09	...	60.8	67.9	75.2	...	53.3	...	56.9	...
Fe I	5216.27	1.61	−2.15	16.6	51.8	65.9	65.7	21.0	50.1	...	51.7	75.1
Fe I	5232.94	2.94	−0.06	29.7	74.5	78.5	90.5	41.9	89.4	...	72.8	75.7
Fe I	5247.05	0.09	−4.95	19.4	35.5
Fe I	5254.96	0.11	−4.76	...	20.8	32.8	30.7	58.7
Fe I	5266.56	3.00	−0.39	...	59.9	62.9	71.7	20.2	72.0	...	54.9	51.6
Fe I	5269.54	0.86	−1.32	...	133.8	138.5	149.1	78.8	118.5	...	130.5	186.9
Fe I	5281.79	3.04	−0.83	...	34.7	34.4	41.5	...	50.8	...	27.1	...
Fe I	5302.30	3.28	−0.72	...	26.2	19.8	41.3
Fe I	5324.18	3.21	−0.10	...	56.7	59.0	74.1	...	75.4	...	60.4	56.1
Fe I	5328.04	0.92	−1.47	...	120.7	130.6	131.2	86.8	111.8	17.0	114.1	172.9
Fe I	5332.90	1.56	−2.78	...	27.0	27.5	38.6
Fe I	5339.93	3.27	−0.65	...	29.6	29.3	44.5	...	47.9	...	33.0	...
Fe I	5341.02	1.61	−1.95	...	66.9	79.1	67.1	...	60.3	...	58.0	...
Fe I	5367.47	4.41	0.44	...	25.2	19.2	50.7	...	44.6
Fe I	5369.96	4.37	0.54	...	29.5	26.3	50.3	...	49.1
Fe I	5371.49	0.96	−1.64	...	109.5	123.8	134.0	81.6	102.8	167.4
Fe I	5383.37	4.31	0.64	...	31.9	34.6	50.6	...	60.9
Fe I	5397.13	0.92	−1.99	...	107.4	...	101.8	72.7	88.5	156.2
Fe I	5404.15	4.43	0.52	...	30.0	68.0
Fe I	5405.77	0.99	−1.84	...	106.6	110.0	122.3	66.0	93.6	155.4
Fe I	5415.20	4.39	0.64	...	29.2	23.3	51.9	...	51.2
Fe I	5424.07	4.32	0.52	...	37.6	33.5	61.8
Fe I	5429.70	0.96	−1.88	73.5	106.6	117.7	108.9	...	89.5	161.3
Fe I	5434.52	1.01	−2.12	48.6	91.4	98.1	100.7	...	85.3
Fe I	5569.62	3.42	−0.54	...	23.6	28.0	47.2	...	17.8	20.9
Fe I	5572.84	3.40	−0.28	...	44.8	38.9	59.4	...	36.4	32.8

Table 4—Continued

Species	Wavelength (Å)	L.E.P. (eV)	$\log gf$	W_λ (mÅ)								
				(1)	(2)	(3)	(4)	(5)	(6)	(7)	(8)	(9)
Fe I	5576.09	3.43	−1.00	...	21.4	16.4	29.7
Fe I	5586.75	3.37	−0.10	13.6	44.8	53.0	72.2	...	70.8	...	43.2	...
Fe I	5615.64	3.33	0.05	30.8	59.2	66.6	...	21.3	81.9	...	62.0	57.5
Fe I	5624.54	3.42	−0.75	...	19.2	21.9	33.2	...	15.7	...
Fe I	6065.48	2.61	−1.53	...	30.0	31.0	31.6	33.4
Fe I	6136.61	2.45	−1.40	46.4	44.1	...
Fe I	6137.69	2.59	−1.40	29.7	...
Fe I	6191.56	2.43	−1.42	...	42.4	48.7	47.9	...	36.4	...
Fe I	6213.43	2.22	−2.48	...	10.1	10.5
Fe I	6219.28	2.20	−2.43	...	14.0	21.6
Fe I	6230.72	2.56	−1.28	...	46.7	48.3	60.2	...	53.9	...	41.2	52.2
Fe I	6393.60	2.43	−1.43	...	42.3	43.8	44.1
Ni I	3858.30	0.42	−0.95	26.2
Ni I	4714.42	3.38	0.23	...	25.6	27.3	43.5	...	29.6	...
Ni I	4980.16	3.61	−0.11	...	12.8	23.9	...	13.1	...
Zn I	4722.15	4.03	−0.39	...	10.7	44.7	...	20.4	...
Zn I	4810.53	4.08	−0.17	...	14.7	21.4	33.3	...	26.4	...	28.8	...
Sc II	4246.82	0.31	0.24	35.2
Sc II	4320.75	0.61	−0.25	53.3	...
Sc II	4400.39	0.61	−0.54	36.1	...
Sc II	4415.54	0.60	−0.67	...	51.8	57.4	...	33.1	55.1	...	39.4	63.7
Sc II	5031.01	1.36	−0.40	...	23.1	26.7	29.7	37.1
Sc II	5526.79	1.77	0.02	...	21.8	30.0	39.5	36.4
Ti II	3913.48	1.12	−0.53	46.8
Ti II	4417.71	1.16	−1.43	36.9	80.7	88.6	...	48.3	71.1	...	74.5	89.4
Ti II	4418.31	1.24	−1.99	...	38.0	47.9	28.9	...	31.6	31.4
Ti II	4441.73	1.18	−2.41	...	26.7	29.7
Ti II	4443.77	1.08	−0.70	59.5	103.8	99.9	...	76.1	102.2	41.5	89.8	128.6
Ti II	4444.54	1.12	−2.21	...	32.2	31.1	48.3
Ti II	4450.50	1.08	−1.51	24.7	73.8	77.1	...	45.8	63.9	...	65.5	86.6
Ti II	4464.46	1.16	−2.08	...	54.8	61.5	37.0	...	49.0	...
Ti II	4468.52	1.13	−0.60	60.8	102.7	111.7	...	88.9	99.4	...	104.5	142.2
Ti II	4501.27	1.12	−0.76	56.0	97.1	103.3	...	71.4	93.4	...	93.6	116.3
Ti II	4529.48	1.57	−2.03	...	35.0	40.6	31.1	...	25.7	...
Ti II	4533.97	1.24	−0.77	53.4	103.6	108.0	...	78.7	101.0	33.4	95.9	120.6
Ti II	4563.77	1.22	−0.96	48.0	91.3	99.5	...	63.6	88.4	27.6	89.2	99.1
Ti II	4571.96	1.57	−0.53	46.9	96.2	102.5	...	62.8	100.6	29.4	87.8	119.8
Ti II	4589.92	1.24	−1.79	...	58.0	56.4	51.1	...	41.8	58.6
Ti II	4779.98	2.05	−1.37	...	29.1	29.9	29.8	...	25.9	...

Table 4—Continued

Species	Wavelength (Å)	L.E.P. (eV)	$\log gf$	W_λ (mÅ)								
				(1)	(2)	(3)	(4)	(5)	(6)	(7)	(8)	(9)
Ti II	4798.51	1.08	−2.67	...	20.7	25.6
Ti II	4805.09	2.06	−1.10	...	41.2	43.3	45.9	...	28.1	32.3
Ti II	5129.15	1.89	−1.39	...	33.0	32.4	33.1	30.6
Ti II	5185.90	1.89	−1.35	...	26.0	23.4	46.8	...	27.9	...	28.1	...
Ti II	5336.78	1.58	−1.63	...	37.8	35.4	78.4	...	34.5	...	29.4	37.5
Ti II	5381.01	1.57	−1.97	...	22.7	20.9	58.5	...	24.9
Ti II	5418.75	1.58	−2.11	...	18.5	14.2	66.0	...	13.8
Fe II	4416.82	2.78	−2.60	...	34.6	36.5	55.9	...	25.8	...
Fe II	4508.28	2.86	−2.58	...	42.6	43.3	48.1	...	38.6	...
Fe II	4515.34	2.84	−2.48	...	29.8	35.3	40.9	...	23.6	...
Fe II	4520.23	2.81	−2.60	...	30.4	34.7	42.1	...	24.3	...
Fe II	4541.52	2.86	−3.05	...	17.7
Fe II	4582.83	2.84	−3.10	...	11.2
Fe II	4583.83	2.81	−2.02	20.2	65.0	67.4	...	34.4	77.2	12.0	53.8	61.4
Fe II	4731.44	2.89	−3.36	...	13.1	23.4
Fe II	4923.93	2.89	−1.32	39.5	83.2	93.5	...	43.7	93.1	23.6	77.1	88.1
Fe II	5018.45	2.89	−1.22	48.7	92.5	97.3	...	69.6	100.0	...	93.5	97.5
Fe II	5169.00	2.89	−0.87	37.2
Fe II	5197.56	3.23	−2.10	32.8	21.3	...
Fe II	5234.62	3.22	−2.27	...	32.2	33.7	45.7	...	44.6	...	29.6	...
Fe II	5276.00	3.20	−1.94	...	36.7	38.1	57.0	...	53.3	...	44.0	27.4
Fe II	5534.83	3.24	−2.93	19.9
Ba II	4130.65	2.72	0.56	54.2
Ba II	4554.03	0.00	0.16	43.8	112.1	125.1	...	111.9	209.2	179.8	78.5	...
Ba II	4934.09	0.00	−0.16	28.6	106.5	121.4	...	120.5	177.4	170.1	67.1	197.4
Ba II	5853.67	0.60	−1.02	...	13.9	24.1	151.2	29.1	80.7	68.2	...	98.7
Ba II	6141.70	0.70	−0.07	21.0	...
Ba II	6496.90	0.60	−0.37	...	48.4	57.0	239.9	77.3	131.9	113.0	...	161.8

Table 5. EQUIVALENT WIDTHS

Species	Wavelength (Å)	L.E.P. (eV)	$\log gf$	W_λ (mÅ)								
				(10)	(11)	(12)	(13)	(14)	(15)	(16)	(17)	(18)
Na I	5682.63	2.10	−0.70	36.0
Na I	5688.20	2.10	−0.46	14.9	34.2	...	60.6
Na I	5889.95	0.00	0.10	156.6	166.8	218.6	200.6	225.6	186.9	295.2	154.9	202.6
Na I	5895.92	0.00	−0.20	151.3	151.6	202.3	178.0	216.0	169.0	246.3	143.2	183.4
Mg I	4571.10	0.00	−5.69	37.0	64.3	80.1	55.9	103.4
Mg I	4702.99	4.35	−0.52	...	73.3	46.0
Mg I	5172.69	2.71	−0.38	177.0	180.1	177.6	175.3	...	173.2	...	133.1	189.0
Mg I	5183.60	2.72	−0.16	229.4	236.9	144.5	...
Mg I	5528.40	4.35	−0.49	...	77.6	...	110.0	102.0	77.1	163.4	44.5	...
Ca I	4425.44	1.88	−0.36	...	49.5	71.9
Ca I	4455.89	1.90	−0.53	...	42.5	81.3	59.4
Ca I	5265.56	2.52	−0.11	...	23.4	27.8
Ca I	5581.97	2.52	−0.56	20.4
Ca I	5588.76	2.53	0.36	...	43.0	...	55.1	62.0	48.9	117.2	...	50.2
Ca I	5594.47	2.52	0.10	54.0	34.6	30.0	54.6	63.2	38.3	128.2	...	46.5
Ca I	5601.29	2.53	−0.52	...	12.2	16.8	17.5
Ca I	5857.45	2.93	0.24	28.1	32.0	39.0	24.8	98.2
Ca I	6102.72	1.88	−0.77	24.9	...	40.5
Ca I	6122.22	1.89	−0.32	67.2	61.7	70.5	63.8	137.7
Ca I	6162.17	1.90	−0.09	78.1	73.1	99.1	73.0	159.2	45.3	...
Ti I	4533.24	0.85	0.53	...	52.6	50.4	47.8	84.9
Ti I	4981.73	0.85	0.56	...	54.2	59.2	55.2	128.3	28.0	...
Ti I	4991.07	0.84	0.44	49.8	44.5	63.7	54.0	126.1
Ti I	4999.50	0.83	0.31	...	39.2	57.2
Ti I	5007.21	0.82	0.17	...	39.0	59.8	49.8	130.6
Ti I	5016.16	0.85	−0.52	18.6
Ti I	5173.74	0.00	−1.06	...	18.9	34.9	37.7
Ti I	5192.97	0.02	−0.95	...	25.9	25.5	39.2	...	52.0
Ti I	5206.08	2.49	1.07	60.7
Ti I	5210.38	0.05	−0.83	33.2	29.5	23.4	46.6	37.7	35.2	102.3	...	34.3
Cr I	4616.14	0.98	−1.19	29.2
Cr I	4626.19	0.97	−1.32	25.2
Cr I	4646.17	1.03	−0.70	50.9	29.4
Cr I	4651.29	0.98	−1.46	27.3
Cr I	4652.16	1.00	−1.03	31.9	22.3
Cr I	5208.44	0.94	0.16	88.9	...	74.0	102.3	109.9	39.3	93.3
Cr I	5298.27	0.98	−1.15	25.1
Cr I	5409.79	1.03	−0.72	41.2	35.7	...	57.1	56.0	38.6	111.6
Fe I	4408.41	2.20	−1.77	...	32.3

Table 5—Continued

Species	Wavelength (Å)	L.E.P. (eV)	$\log gf$	W_λ (mÅ)								
				(10)	(11)	(12)	(13)	(14)	(15)	(16)	(17)	(18)
Fe I	4422.57	2.85	−1.11	...	29.9
Fe I	4430.61	2.22	−1.66	...	43.4	63.2
Fe I	4442.34	2.20	−1.25	...	64.6
Fe I	4443.19	2.86	−1.04	...	33.8
Fe I	4447.72	2.22	−1.34	...	53.7	83.0
Fe I	4461.65	0.09	−3.21	...	92.9	96.7	106.7
Fe I	4466.55	2.83	−0.60	60.4	58.8	81.0	58.8	109.7
Fe I	4476.02	2.85	−0.82	54.9	54.3	88.1	53.1	127.8
Fe I	4484.22	3.60	−0.86	62.5
Fe I	4489.74	0.12	−3.97	...	57.5	60.8	66.3	104.0
Fe I	4494.56	2.20	−1.14	71.7	71.5	83.7	75.5
Fe I	4528.61	2.18	−0.82	...	92.2	111.4	...	71.7	...
Fe I	4531.15	1.49	−2.15	...	64.8	70.1	...	47.0	...
Fe I	4592.65	1.56	−2.45	33.4	43.2	71.1	56.3	111.7
Fe I	4602.94	1.49	−2.21	...	59.3	68.4	63.7	101.9
Fe I	4733.59	1.49	−2.99	38.0
Fe I	4736.77	3.21	−0.75	...	34.8	54.7
Fe I	4871.32	2.87	−0.36	82.7	68.7	82.5	71.8	133.3
Fe I	4872.14	2.88	−0.57	...	55.4	70.8	68.7	142.4
Fe I	4890.75	2.88	−0.39	...	65.0	96.2	77.3
Fe I	4891.49	2.85	−0.11	...	86.6	86.8	95.3	158.4	54.2	...
Fe I	4903.31	2.88	−0.93	...	36.6	59.3	43.0	92.4
Fe I	4918.99	2.87	−0.34	...	61.5	79.7	77.8	134.1
Fe I	4920.50	2.83	0.07	...	92.5	197.9	53.6	...
Fe I	4924.77	2.28	−2.26	...	17.2	28.2	33.0	83.3
Fe I	4938.81	2.88	−1.08	...	39.6	48.3	34.6	85.7
Fe I	4939.69	0.86	−3.34	...	51.8	44.1	68.8
Fe I	4994.13	0.92	−2.96	60.3	52.8	64.5	64.0	100.1
Fe I	5006.12	2.83	−0.61	...	57.5	71.6	62.0	...	48.2	...
Fe I	5012.07	0.86	−2.64	64.6	87.1	79.6	79.5	131.6
Fe I	5041.76	1.49	−2.20	...	73.3	81.9	78.2	...	16.7	...
Fe I	5049.82	2.28	−1.34	...	56.6	73.7	60.3
Fe I	5051.63	0.92	−2.80	...	76.4	77.3	77.0	121.0	26.9	...
Fe I	5068.77	2.94	−1.04	...	29.0	54.9	31.2
Fe I	5083.34	0.96	−2.96	...	63.8	77.2	66.1
Fe I	5110.41	0.00	−3.76	...	91.8	88.6
Fe I	5123.72	1.01	−3.07	...	51.5	75.1
Fe I	5127.36	0.92	−3.31	...	49.5	52.2	44.4
Fe I	5133.69	4.18	0.14	...	24.3	51.4	36.8

Table 5—Continued

Species	Wavelength (Å)	L.E.P. (eV)	$\log gf$	(10)	(11)	(12)	(13)	W_λ (mÅ)	(14)	(15)	(16)	(17)	(18)
Fe I	5150.84	0.99	−3.00	...	53.5	48.4	50.6
Fe I	5151.91	1.01	−3.32	...	40.4	45.3	48.4
Fe I	5162.27	4.18	0.02	...	27.7	43.9	17.1
Fe I	5166.28	0.00	−4.20	49.0	58.5	...	60.0	58.8	61.8	104.9	...	77.2	...
Fe I	5171.60	1.49	−1.79	73.3	84.5	69.4	81.8	94.3	89.8	127.5	69.3	91.2	...
Fe I	5191.46	3.04	−0.55	...	54.7	100.2	68.9
Fe I	5192.34	3.00	−0.42	55.1	57.9	44.1	75.9	...	71.4	...	28.1
Fe I	5194.94	1.56	−2.09	54.0	73.7	42.5	78.2	...	71.7
Fe I	5216.27	1.61	−2.15	53.6	55.9	34.9	57.8	68.1	68.2	118.3	...	51.7	...
Fe I	5232.94	2.94	−0.06	71.6	70.7	64.5	79.9	...	78.7	139.7	43.2	105.0	...
Fe I	5247.05	0.09	−4.95	16.3	53.1
Fe I	5254.96	0.11	−4.76	12.6	24.7	30.5	81.4
Fe I	5266.56	3.00	−0.39	53.0	56.7	44.2	66.8	81.0	65.1	121.2	28.0	71.3	...
Fe I	5269.54	0.86	−1.32	115.8	138.4	123.3	139.8	143.3	139.5	...	88.0	142.9	...
Fe I	5281.79	3.04	−0.83	30.8	37.3	...	43.2	52.4	36.7	96.8	...	50.3	...
Fe I	5302.30	3.28	−0.72	...	26.9	42.5	30.5
Fe I	5324.18	3.21	−0.10	60.5	58.7	47.1	...	83.4	60.9	122.3	...	74.6	...
Fe I	5328.04	0.92	−1.47	107.5	127.1	108.7	126.2	128.8	130.1	181.8	81.1
Fe I	5332.90	1.56	−2.78	...	34.2	40.3	34.8	80.2
Fe I	5339.93	3.27	−0.65	29.7	35.8	...	49.3	...	33.6
Fe I	5341.02	1.61	−1.95	55.6	76.3	...	71.2	...	73.9	133.5
Fe I	5367.47	4.41	0.44	33.4	44.9	37.6	24.9
Fe I	5369.96	4.37	0.54	37.5	26.7	...	43.5	40.5	27.5	100.7
Fe I	5371.49	0.96	−1.64	111.5	125.9	115.4	132.3	122.9	118.7	...	73.8
Fe I	5383.37	4.31	0.64	...	33.5	54.2	31.1
Fe I	5397.13	0.92	−1.99	90.0	...	100.6	114.7	144.7	68.4
Fe I	5404.15	4.43	0.52	...	43.5	56.3	35.2
Fe I	5405.77	0.99	−1.84	99.9	107.8	98.3	111.9	122.8	112.1	150.9	55.1
Fe I	5415.20	4.39	0.64	41.1	29.8	...	50.1	40.7	30.1	95.1
Fe I	5424.07	4.32	0.52	...	41.6	55.2	39.7
Fe I	5429.70	0.96	−1.88	88.9	123.0	88.3	104.1	109.5	113.0	...	50.5
Fe I	5434.52	1.01	−2.12	85.3	103.8	91.2	112.4	...	100.9
Fe I	5569.62	3.42	−0.54	...	28.8	46.8	31.1
Fe I	5572.84	3.40	−0.28	...	41.8	64.2	43.6
Fe I	5576.09	3.43	−1.00	35.0	25.6
Fe I	5586.75	3.37	−0.10	48.2	49.7	74.3	51.7	109.4
Fe I	5615.64	3.33	0.05	...	59.1	76.9	64.5	149.5	29.6
Fe I	5624.54	3.42	−0.75	37.7	16.6
Fe I	6065.48	2.61	−1.53	51.5	61.1	38.7	102.9

Table 5—Continued

Species	Wavelength (Å)	L.E.P. (eV)	$\log gf$	W_λ (mÅ)								
				(10)	(11)	(12)	(13)	(14)	(15)	(16)	(17)	(18)
Fe I	6136.61	2.45	−1.40	47.2	52.2
Fe I	6191.56	2.43	−1.42	38.4	49.1	54.2	53.1
Fe I	6213.43	2.22	−2.48	32.3	15.6	75.8
Fe I	6219.28	2.20	−2.43	18.6	46.7	23.2	78.7
Fe I	6230.72	2.56	−1.28	44.9	51.8	34.8	48.5	60.8	51.1	108.4
Fe I	6393.60	2.43	−1.43	46.0	50.5	...	74.1	74.6	44.2	123.6	19.5	...
Ni I	4714.42	3.38	0.23	...	25.5	40.0	31.1
Ni I	4980.16	3.61	−0.11	14.8	67.3
Zn I	4722.15	4.03	−0.39	...	17.2	16.8
Zn I	4810.53	4.08	−0.17	27.3	15.1	16.1	20.1	62.6
Sc II	4415.54	0.60	−0.67	100.4	64.1	66.1	93.2	106.7
Sc II	5031.01	1.36	−0.40	...	31.6	37.2	31.4
Sc II	5526.79	1.77	0.02	...	29.3	61.2	35.0
Ti II	4417.71	1.16	−1.43	...	96.2	94.6
Ti II	4418.31	1.24	−1.99	...	44.3	55.0	61.1
Ti II	4441.73	1.18	−2.41	...	36.3	43.5
Ti II	4443.77	1.08	−0.70	106.7	110.4	114.5	118.5	151.5	65.0	...
Ti II	4444.54	1.12	−2.21	...	33.9
Ti II	4450.50	1.08	−1.51	...	83.1	73.0	83.0
Ti II	4464.46	1.16	−2.08	71.2	57.4	61.1	64.4
Ti II	4468.52	1.13	−0.60	...	100.3	116.4	114.4
Ti II	4501.27	1.12	−0.76	99.0	109.2	103.8	104.7	...	65.2	...
Ti II	4529.48	1.57	−2.03	...	37.1	53.9
Ti II	4533.97	1.24	−0.77	...	104.4	100.7	128.9
Ti II	4563.77	1.22	−0.96	109.0	98.4	99.9	109.2	142.7	62.3	...
Ti II	4571.96	1.57	−0.53	...	98.8	109.5	111.1
Ti II	4589.92	1.24	−1.79	43.9	61.1	67.5	58.0	78.5
Ti II	4779.98	2.05	−1.37	44.7	31.7	36.4	...	74.3
Ti II	4798.51	1.08	−2.67	...	23.6	25.1
Ti II	4805.09	2.06	−1.10	68.1	38.0	50.8	48.2	100.0
Ti II	5129.15	1.89	−1.39	43.2
Ti II	5185.90	1.89	−1.35	...	33.7	26.4	41.6	35.7	33.1	68.9	...	29.2
Ti II	5336.78	1.58	−1.63	...	38.8	47.2	46.3
Ti II	5381.01	1.57	−1.97	47.5	40.4	32.1
Ti II	5418.75	1.58	−2.11	27.0	82.0
Fe II	4416.82	2.78	−2.60	...	37.7	66.1	56.5
Fe II	4508.28	2.86	−2.58	...	47.0	43.9	48.3	78.1
Fe II	4515.34	2.84	−2.48	...	26.9
Fe II	4520.23	2.81	−2.60	37.0

Table 5—Continued

Species	Wavelength (Å)	L.E.P. (eV)	$\log gf$	W_λ (mÅ)								
				(10)	(11)	(12)	(13)	(14)	(15)	(16)	(17)	(18)
Fe II	4582.83	2.84	−3.10	23.4
Fe II	4583.83	2.81	−2.02	53.9	79.7	76.2	74.6	...	51.1	...
Fe II	4731.44	2.89	−3.36	17.5	24.9	44.9
Fe II	4923.93	2.89	−1.32	89.0	93.8	91.6	92.8	132.8	53.0	...
Fe II	5018.45	2.89	−1.22	...	102.0	104.8	101.0	...	57.5	...
Fe II	5197.56	3.23	−2.10	...	29.7	...	37.8	68.7	...	25.6
Fe II	5234.62	3.22	−2.27	29.4	39.2	17.6	38.2	48.5	38.6	73.9	...	52.2
Fe II	5276.00	3.20	−1.94	38.2	43.6	35.6	...	49.7	52.9	98.9	...	52.5
Fe II	5534.83	3.24	−2.93	16.9	16.7
Ba II	4554.03	0.00	0.16	...	110.3	204.3	...	129.3	...
Ba II	4934.09	0.00	−0.16	...	104.5	222.3	259.6	...	222.3	...	141.4	275.0
Ba II	5853.67	0.60	−1.02	118.3	19.4	122.5	122.4	113.5	96.2	188.1	52.5	153.3
Ba II	6141.70	0.70	−0.07	169.3	...	327.0	...	201.1
Ba II	6496.90	0.60	−0.37	181.9	48.8	212.3	197.8	182.1	146.5	260.1	80.5	241.8

Table 6. EQUIVALENT WIDTHS

Species	Wavelength (Å)	L.E.P. (eV)	$\log gf$	W_λ (mÅ)							
				(19)	(20)	(21)	(22)	(23)	(24)	(25)	(26)
Na I	5889.95	0.00	0.10	...	228.5	171.7	...	170.8	...	292.6	166.6
Na I	5895.92	0.00	−0.20	246.6	211.5	149.7	213.9	162.2	246.5	275.9	142.8
Mg I	4571.10	0.00	−5.69	33.0
Mg I	4702.99	4.35	−0.52	67.0
Mg I	5172.69	2.71	−0.38	297.7	187.9	192.1	216.7	170.4	272.2	183.4	163.8
Mg I	5183.60	2.72	−0.16	182.5
Mg I	5528.40	4.35	−0.49	114.0	53.5
Ca I	5588.76	2.53	0.36	119.2	80.1	52.3	31.8
Ca I	5594.47	2.52	0.10	119.9	48.7	...	72.5	...	90.5	56.1	30.4
Ca I	5601.29	2.53	−0.52	28.9
Ca I	5857.45	2.93	0.24	37.5	63.0	...	81.5	35.6	22.2
Ca I	6102.72	1.88	−0.77	98.1	54.2	30.4	15.0
Ca I	6122.22	1.89	−0.32	66.1	45.3
Ca I	6162.17	1.90	−0.09	...	123.1	95.7	...	94.5	149.1	68.9	58.9
Ti I	4981.73	0.85	0.56	44.0
Ti I	5192.97	0.02	−0.95	...	43.7	...	56.8	...	105.5	44.0	...
Ti I	5206.08	2.49	1.07	126.1	87.0	70.2	...	65.7
Ti I	5210.38	0.05	−0.83	103.1	49.2	31.7	64.2	...	122.6	40.1	...
Cr I	5208.44	0.94	0.16	102.8	...	95.1	...	86.4	75.8
Cr I	5409.79	1.03	−0.72	51.1	...
Fe I	4461.65	0.09	−3.21	88.7
Fe I	4489.74	0.12	−3.97	46.7
Fe I	4528.61	2.18	−0.82	72.3
Fe I	4871.32	2.87	−0.36	61.7
Fe I	4890.75	2.88	−0.39	77.3	58.4
Fe I	4891.49	2.85	−0.11	74.3
Fe I	4920.50	2.83	0.07	73.9
Fe I	4924.77	2.28	−2.26	20.8
Fe I	4994.13	0.92	−2.96	37.5
Fe I	5012.07	0.86	−2.64	60.8
Fe I	5051.63	0.92	−2.80	45.0
Fe I	5110.41	0.00	−3.76	60.2
Fe I	5166.28	0.00	−4.20	144.8	82.3	...	85.3	44.5	146.1	37.0	24.1
Fe I	5171.60	1.49	−1.79	140.0	97.6	66.9	97.3	87.4	146.1	67.5	58.4
Fe I	5191.46	3.04	−0.55	...	89.0	36.1
Fe I	5192.34	3.00	−0.42	...	76.3	...	87.3	49.9	105.2	54.7	51.6
Fe I	5194.94	1.56	−2.09	150.5	77.1	59.9	80.6	...	126.8	51.1	49.0
Fe I	5216.27	1.61	−2.15	126.5	71.0	37.5	68.3	44.4	106.7	44.1	43.7
Fe I	5232.94	2.94	−0.06	129.9	94.9	61.5	93.8	53.8	121.8	68.3	59.3

Table 6—Continued

Species	Wavelength (Å)	L.E.P. (eV)	$\log gf$	W_λ (mÅ)							
				(19)	(20)	(21)	(22)	(23)	(24)	(25)	(26)
Ti II	4571.96	1.57	−0.53	93.1
Ti II	4589.92	1.24	−1.79	38.0
Ti II	4779.98	2.05	−1.37	21.0
Ti II	5185.90	1.89	−1.35	85.2	50.7	31.7	55.7	...	76.7	21.1	...
Ti II	5336.78	1.58	−1.63	56.5	...
Ti II	5381.01	1.57	−1.97	35.3	...
Fe II	4508.28	2.86	−2.58	27.4
Fe II	4583.83	2.81	−2.02	51.2
Fe II	4923.93	2.89	−1.32	84.7
Fe II	5018.45	2.89	−1.22	84.6
Fe II	5197.56	3.23	−2.10	96.2	39.5	37.4	49.9	...	66.5	...	21.1
Fe II	5234.62	3.22	−2.27	69.5	48.9	28.9	57.9	...	63.9	25.5	...
Fe II	5276.00	3.20	−1.94	92.9	47.7	51.3	62.0	41.2	...	28.7	29.1
Ba II	4554.03	0.00	0.16	...	252.5	267.1	169.5
Ba II	4934.09	0.00	−0.16	...	261.0	...	267.3	168.8
Ba II	5853.67	0.60	−1.02	219.4	141.3	136.8	143.0	128.8	64.2
Ba II	6141.70	0.70	−0.07	285.6	164.4	233.5	189.8	182.2
Ba II	6496.90	0.60	−0.37	219.9	...	188.6	256.6	182.6	111.7

Table 7. EQUIVALENT WIDTHS

Species	Wavelength (Å)	L.E.P. (eV)	$\log gf$	W_λ (mÅ) CS 22958–028
Fe I	3618.77	0.99	0.00	68.4
Fe I	3631.46	0.96	−0.04	47.5
Fe I	3745.56	0.09	−0.77	65.0
Fe I	3758.23	0.96	−0.03	52.2
Fe I	3815.84	1.49	0.23	65.1
Fe I	3820.43	0.86	0.12	92.4
Fe I	3824.44	0.00	−1.36	44.0
Fe I	3825.88	0.92	−0.04	76.5
Fe I	3827.82	1.56	0.06	48.2
Fe I	3849.97	1.01	−0.87	39.5
Fe I	3856.37	0.05	−1.29	40.1
Fe I	3859.91	0.00	−0.71	80.3
Fe I	3865.52	1.01	−0.98	33.3
Fe I	3899.71	0.09	−1.53	45.3
Fe I	3920.26	0.12	−1.75	36.4
Fe I	3922.91	0.05	−1.65	36.5
Fe I	3930.30	0.09	−1.49	37.7
Fe I	4005.24	1.56	−0.61	30.3
Fe I	4045.81	1.49	0.28	69.3
Fe I	4071.74	1.61	−0.02	53.5
Fe I	4132.06	1.61	−0.67	20.9
Fe I	4143.87	1.56	−0.51	31.4
Fe I	4202.03	1.49	−0.71	22.3
Fe I	4260.47	2.40	0.08	30.6
Fe I	4325.76	1.61	0.01	56.7
La II	3849.02	0.00	−0.45	33.4
La II	3949.10	0.40	0.49	82.5
La II	3988.52	0.40	0.21	53.4
La II	3995.75	0.17	−0.06	36.7
La II	4123.23	0.32	0.13	32.0
La II	4286.97	1.95	0.21	36.0

Table 7—Continued

Species	Wavelength (Å)	L.E.P. (eV)	$\log gf$	W_λ (mÅ) CS 22958–028
La II	4333.74	0.17	−0.06	43.3
Ce II	4186.60	0.86	0.90	35.3
Nd II	4156.08	0.18	0.10	29.7

Table 8. EQUIVALENT WIDTHS OF Na LINES

Species	Wavelength (Å)	L.E.P. (eV)	$\log gf$	W_λ (mÅ)								
				(Na1)	(Na2)	(Na3)	(Na4)	(Na5)	(Na6)	(Na7)	(Na8)	(Na9)
Na I	5682.63	2.10	−0.70	3.4
Na I	5688.20	2.10	−0.46	8.6	6.1
Na I	5889.95	0.00	0.10	186.7	146.3	116.6	151.4	128.9	171.3	84.1	220.3	...
Na I	5895.92	0.00	−0.20	165.2	122.3	100.8	133.8	99.9	155.0	...	197.8	...

Table 9. ATMOSPHERIC PARAMETERS

ID	Object	T_{eff} (K)	$\log g$	[Fe/H]	v_{micr} (km ⁻¹)
1	BS 16929–005	5250	2.8	–3.2	2.3
2	CS 22174–007	5300	2.7	–2.3	2.1
3	CS 22886–042	4800	1.6	–2.5	2.1
4	CS 22948–027	5000	1.9	–2.3	2.0
5	CS 22960–053	5200	2.1	–3.2	2.1
6	CS 29503–010	6500	4.5	–1.2	1.9
7	CS 29528–028	6800	4.0	–2.9	1.9
8	CS 30312–100	5300	2.8	–2.4	2.2
9	CS 30322–023	4300	1.0	–3.3	3.3
10	CS 30338–089	5000	2.1	–2.5	1.7
11	CS 31062–041	5100	2.2	–2.5	2.3
12	CS 29497–034	4900	1.5	–3.0	2.2
13	HE 0206–1916	5200	2.7	–2.2	2.0
14	HE 0400–2030	5600	3.5	–1.8	2.2
15	HE 0441–0652	4900	1.4	–2.5	2.3
16	HE 0507–1653	5000	2.4	–1.5	2.0 ^a
17	HE 1005–1439	5000	1.9	–3.2	2.0
18	HE 1157–0518	4900	2.0	–2.4	2.0 ^a
19	HE 1319–1935	4600	1.1	–1.8	2.0 ^a
20	HE 1429–0551	4700	1.5	–2.5	2.0
21	HE 1447+0102	5100	1.7	–2.5	1.8
22	HE 1523–1155	4800	1.6	–2.2	1.8
23	HE 1528–0409	5000	1.8	–2.6	1.8
24	HE 2221–0453	4400	0.4	–2.2	2.0 ^a
25	HE 2228–0706	5100	2.6	–2.5	1.6
26	HE 2330–0555	4900	1.7	–2.8	1.8

^aassumed values (see text)

Table 10. ABUNDANCE RESULTS

	Fe (Fe I) ^a	Fe (Fe II) ^a	C ^b	N ^b	Na	Mg	Ca	Sc	Ti (Ti I)	Ti (Ti II)	Cr	Ni	Zn	Ba
$\log \epsilon_{\text{Sun}}^c$	7.45	7.45	8.39	7.78	6.17	7.53	6.31	3.05	4.90	4.90	5.64	6.23	4.60	2.17
BS 16920–005														
$\log \epsilon$	4.28	4.27	6.3	< 7.0	2.94	4.85	3.27	2.17	2.14	−1.48
[X/Fe]	−3.17	−3.18	1.08	<2.39	−0.06	0.49	0.13	0.44	−0.34	−0.48
<i>N</i>	24	3	CH4322	CN4215	2	4	2	8	1	2
s.e.([X/Fe])	0.14	0.13	0.16	0.07	0.17	0.10	0.09	0.14	0.09	0.12
CS 22174–007														
$\log \epsilon$	5.26	5.26	6.6	< 7.0	4.36	5.82	4.35	0.96	3.09	3.17	3.26	4.07	2.46	−0.59
[X/Fe]	−2.20	−2.20	0.41	<1.42	0.39	0.49	0.24	0.11	0.39	0.46	−0.19	0.03	0.06	−0.57
<i>N</i>	85	12	CH4322	CN4215	2	5	10	3	8	22	7	2	2	4
s.e.([X/Fe])	0.14	0.13	0.16	0.07	0.17	0.10	0.10	0.14	0.09	0.14	0.09	0.11	0.13	0.13
CS 22886–042														
$\log \epsilon$	4.84	4.84	5.9	< 7.2	3.91	5.43	3.96	0.48	2.45	2.63	2.74	3.65	2.28	−0.94
[X/Fe]	−2.61	−2.61	0.12	<2.03	0.35	0.51	0.26	0.04	0.16	0.35	−0.29	0.03	0.29	−0.50
<i>N</i>	84	10	CH4322	CN4215	2	5	10	3	8	21	3	1	1	4
s.e.([X/Fe])	0.14	0.13	0.16	0.07	0.17	0.10	0.10	0.14	0.09	0.13	0.09	0.11	0.13	0.13
CS 22948–027														
$\log \epsilon$	5.24	5.22	8.3	8.0	4.88	5.87	4.67	...	3.28	3.37	3.31	...	2.69	2.27
[X/Fe]	−2.21	−2.23	2.12	2.43	0.92	0.55	0.57	...	0.60	0.68	−0.12	...	0.31	2.31
<i>N</i>	25	2	CC5635	CN4215	2	1	5	...	3	4	2	...	1	2
s.e.([X/Fe])	0.28	0.16	0.20	0.35	0.13	0.14	0.19	...	0.13	0.26	0.12	...	0.21	0.15
CS 22960–053														
$\log \epsilon$	4.31	4.30	7.3	7.7	...	5.04	3.61	0.40	...	2.30	2.27	−0.11
[X/Fe]	−3.14	−3.15	2.05	3.06	...	0.65	0.43	0.49	...	0.54	−0.23	0.86
<i>N</i>	16	3	CH4322	CN4215	...	3	2	1	...	8	1	4
s.e.([X/Fe])	0.15	0.15	0.16	0.21	...	0.12	0.12	0.15	...	0.15	0.11	0.14
CS 29503–010														
$\log \epsilon$	6.39	6.34	8.4	< 8.0	5.23	6.83	5.41	2.30	4.23	4.23	4.46	5.18	3.85	2.61
[X/Fe]	−1.06	−1.11	1.07	<1.28	0.12	0.36	0.16	0.31	0.39	0.39	−0.12	0.01	0.32	1.50
<i>N</i>	74	11	CH4322	CN4215	2	2	12	3	5	20	2	2	1	4

Table 10—Continued

	Fe (Fe I) ^a	Fe (Fe II) ^a	C ^b	N ^b	Na	Mg	Ca	Sc	Ti (Ti I)	Ti (Ti II)	Cr	Ni	Zn	Ba
s.e.([X/Fe])	0.19	0.17	0.19	0.09	0.15	0.18	0.15	0.14	0.22	0.17	0.10	0.12	0.11	0.16
CS 29528–028														
log ϵ	4.59	4.57	8.3	<8.5	6.05	6.36	3.91	0.78	...	2.91	...	3.63	...	2.58
[X/Fe]	−2.86	−2.88	2.77	<3.58	2.74	1.69	0.46	0.59	...	0.87	...	0.26	...	3.27
N	28	3	CH4322	CN4215	3	3	1	1	...	5	...	1	...	5
s.e.([X/Fe])	0.22	0.18	0.21	0.16	0.19	0.21	0.19	0.18	...	0.20	...	0.16	...	0.20
CS 30312–100														
log ϵ	5.12	5.12	6.6	< 7.3	4.02	5.66	4.16	0.69	2.96	3.03	3.43	4.11	2.82	−0.94
[X/Fe]	−2.33	−2.33	0.54	<1.85	0.18	0.47	0.18	−0.03	0.40	0.46	0.12	0.21	0.55	−0.78
N	59	10	CH4322	CN4215	2	5	10	3	8	16	3	2	2	3
s.e.([X/Fe])	0.14	0.13	0.16	0.07	0.17	0.10	0.10	0.14	0.09	0.16	0.09	0.11	0.13	0.13
CS 30322–023														
log ϵ	4.20	4.18	5.7	7.0	3.96	4.82	3.36	0.08	1.72	2.00	2.04	−0.49
[X/Fe]	−3.25	−3.28	0.56	2.47	1.04	0.54	0.30	0.28	0.07	0.35	−0.36	0.59
N	53	4	CH4322	CN4215	1	3	5	3	7	14	2	3
s.e.([X/Fe])	0.23	0.18	0.12	0.33	0.18	0.26	0.16	0.18	0.18	0.23	0.15	0.17
CS 30338–089														
log ϵ	5.01	5.00	8.0	6.6	4.45	5.56	4.38	1.86	2.79	3.22	3.19	...	2.62	1.94
[X/Fe]	−2.45	−2.45	2.06	1.27	0.73	0.48	0.51	1.26	0.33	0.77	−0.01	...	0.46	2.22
N	34	4	CC5635	CN4215	3	2	4	1	2	7	2	...	2	2
s.e.([X/Fe])	0.20	0.15	0.19	0.33	0.13	0.14	0.11	0.10	0.13	0.25	0.12	...	0.17	0.15
CS 31062–041														
log ϵ	5.08	5.07	6.6	< 7.0	4.23	5.70	4.15	0.87	2.78	2.95	3.07	3.82	2.42	−0.43
[X/Fe]	−2.37	−2.38	0.58	<1.59	0.43	0.54	0.21	0.19	0.25	0.43	−0.20	−0.04	0.20	−0.23
N	75	9	CH4322	CN4215	2	4	8	3	8	19	1	1	2	4
s.e.([X/Fe])	0.15	0.15	0.16	0.07	0.18	0.12	0.11	0.15	0.11	0.17	0.11	0.12	0.14	0.14
CS 29497–034														
log ϵ	4.54	4.56	8.2	7.5	5.03	5.93	3.91	...	2.51	2.40	2.57	1.49
[X/Fe]	−2.91	−2.89	2.72	2.63	1.78	1.31	0.52	...	0.52	0.41	−0.15	2.23
N	15	2	CC5635	CN4215	2	3	1	...	2	1	1	3

Table 10—Continued

	Fe (Fe I) ^a	Fe (Fe II) ^a	C ^b	N ^b	Na	Mg	Ca	Sc	Ti (Ti I)	Ti (Ti II)	Cr	Ni	Zn	Ba
s.e.([X/Fe])	0.27	0.14	0.20	0.53	0.12	0.12	0.12	...	0.11	0.21	0.10	0.13
HE 0206–1916														
log ϵ	5.36	5.38	8.4	7.3	4.82	5.96	4.33	...	3.22	3.40	3.55	2.05
[X/Fe]	−2.09	−2.08	2.10	1.61	0.74	0.52	0.11	...	0.41	0.58	0.00	1.97
N	22	2	CC5635	CN4215	2	3	4	...	2	2	2	3
s.e.([X/Fe])	0.20	0.16	0.19	0.33	0.14	0.15	0.13	...	0.14	0.19	0.13	0.16
HE 0400–2030														
log ϵ	5.72	5.70	7.8	8.8	5.20	6.42	4.76	1.63	3.44	3.58	3.82	4.40	2.67	2.07
[X/Fe]	−1.73	−1.76	1.14	2.75	0.76	0.62	0.18	0.32	0.27	0.41	−0.08	−0.10	−0.20	1.64
N	66	11	CH4322	CN4215	3	2	9	3	7	18	8	1	1	3
s.e.([X/Fe])	0.17	0.18	0.16	0.31	0.20	0.14	0.14	0.17	0.14	0.17	0.14	0.15	0.16	0.16
HE 0441–0652														
log ϵ	4.98	4.97	7.3	6.2	4.42	5.40	4.15	0.72	2.77	2.71	2.90	3.88	2.29	0.81
[X/Fe]	−2.47	−2.48	1.38	0.89	0.72	0.35	0.31	0.14	0.34	0.29	−0.26	0.12	0.17	1.11
N	74	9	CC5165	CN4215	2	4	9	3	0	17	3	2	2	4
s.e.([X/Fe])	0.20	0.21	0.19	0.24	0.14	0.15	0.13	0.11	0.14	0.20	0.13	0.11	0.18	0.24
HE 0507–1653														
log ϵ	6.07	6.06	8.3	7.2	5.22	6.34	5.51	1.87	3.99	3.90	4.33	5.09	3.34	2.68
[X/Fe]	−1.38	−1.39	1.29	0.80	0.43	0.19	0.58	0.20	0.47	0.38	0.07	0.25	0.12	1.89
N	28	5	CC5635	CN4215	4	1	5	1	5	7	1	1	1	3
s.e.([X/Fe])	0.19	0.17	0.19	0.32	0.29	0.12	0.12	0.17	0.12	0.15	0.12	0.15	0.16	0.14
HE 1005–1439														
log ϵ	4.28	4.30	7.7	6.4	4.19	4.97	3.71	...	2.21	1.92	2.10	0.07
[X/Fe]	−3.17	−3.15	2.48	1.79	1.19	0.60	0.57	...	0.48	0.19	−0.38	1.06
N	19	3	CC5170	CN4215	2	3	1	...	1	3	1	4
s.e.([X/Fe])	0.32	0.22	0.20	0.27	0.21	0.21	0.21	...	0.21	0.28	0.20	0.22
HE 1157–0518														
log ϵ	5.11	5.10	8.2	7.0	4.74	5.69	4.13	...	2.66	2.65	3.02	1.97
[X/Fe]	−2.34	−2.35	2.15	1.56	0.92	0.50	0.16	...	0.10	0.09	−0.28	2.14
N	8	3	CC5635	CN4215	2	1	2	...	1	1	1	4

Table 10—Continued

	Fe (Fe I) ^a	Fe (Fe II) ^a	C ^b	N ^b	Na	Mg	Ca	Sc	Ti (Ti I)	Ti (Ti II)	Cr	Ni	Zn	Ba
s.e.([X/Fe])	0.31	0.19	0.29	0.56	0.18	0.16	0.16	...	0.20	0.23	0.18	0.24
HE 1319–1935														
log ϵ	5.71	5.72	8.1	6.5	4.95	6.26	5.06	...	3.26	3.35	4.65	2.31
[X/Fe]	−1.74	−1.73	1.45	0.46	0.52	0.47	0.50	...	0.10	0.19	0.75	1.89
N	15	3	CC5635	CN4215	1	1	3	...	1	1	1	2
s.e.([X/Fe])	0.33	0.22	0.29	0.56	0.21	0.20	0.20	...	0.23	0.25	0.21	0.26
HE 1429–0551														
log ϵ	4.98	4.97	8.2	6.7	4.84	5.58	4.55	...	2.66	2.80	1.27
[X/Fe]	−2.47	−2.48	2.28	1.39	1.14	0.52	0.70	...	0.23	0.37	1.57
N	17	3	CC5635	CN4215	2	1	2	...	2	1	4
s.e.([X/Fe])	0.20	0.16	0.19	0.52	0.14	0.15	0.12	...	0.13	0.18	0.17
HE 1447+0102														
log ϵ	4.98	5.00	8.4	6.7	4.77	6.50	4.73	...	2.89	2.71	2.40
[X/Fe]	−2.47	−2.45	2.48	1.39	1.07	1.43	0.88	...	0.46	0.27	2.70
N	12	3	CC5635	CN4215	2	1	2	...	1	1	3
s.e.([X/Fe])	0.27	0.14	0.20	0.44	0.12	0.13	0.13	...	0.11	0.22	0.14
HE 1523–1155														
log ϵ	5.30	5.28	8.1	7.3	5.21	6.00	4.63	...	3.07	3.02	1.74
[X/Fe]	−2.15	−2.17	1.86	1.67	1.19	0.62	0.46	...	0.32	0.27	1.72
N	16	3	CC5635	CN4215	1	1	4	...	2	1	3
s.e.([X/Fe])	0.19	0.14	0.19	0.52	0.12	0.15	0.11	...	0.11	0.17	0.14
HE 1528–0409														
log ϵ	4.85	4.86	8.2	7.2	4.69	5.76	4.74	1.87
[X/Fe]	−2.61	−2.59	2.42	2.03	1.13	0.83	1.04	2.30
N	15	1	CC5635	CN4215	2	1	1	3
s.e.([X/Fe])	0.19	0.14	0.19	0.52	0.12	0.13	0.10	0.14
HE 2221–0453														
log ϵ	5.23	5.23	8.0	6.4	4.86	6.10	4.91	...	3.21	2.96	2.87	1.69
[X/Fe]	−2.22	−2.23	1.83	0.84	0.92	0.80	0.82	...	0.54	0.28	0.49	1.75
N	19	2	CC5635	CN4215	1	1	3	...	2	1	1	1

Table 10—Continued

	Fe (Fe I) ^a	Fe (Fe II) ^a	C ^b	N ^b	Na	Mg	Ca	Sc	Ti (Ti I)	Ti (Ti II)	Cr	Ni	Zn	Ba
s.e.([X/Fe])	0.31	0.20	0.31	0.48	0.18	0.17	0.17	...	0.21	0.24	0.26	0.24
HE 2228–0706														
log ϵ	5.04	5.04	8.3	6.5	5.43	5.79	4.37	...	3.13	3.15	3.39	...	2.63	2.26
[X/Fe]	−2.41	−2.42	2.32	1.13	1.67	0.67	0.47	...	0.64	0.66	0.16	...	0.44	2.50
N	30	2	CC5635	CN4215	2	1	6	...	2	3	2	...	1	2
s.e.([X/Fe])	0.20	0.16	0.19	0.33	0.14	0.15	0.13	...	0.14	0.19	0.13	...	0.18	0.16
HE 2330–0555														
log ϵ	4.68	4.69	7.7	6.0	4.37	5.42	3.96	0.53	2.44	2.51	2.77	0.61
[X/Fe]	−2.78	−2.76	2.09	1.00	0.97	0.67	0.42	0.25	0.31	0.39	−0.10	1.22
N	40	6	CC5635	CN4215	2	5	7	2	1	7	1	4
s.e.([X/Fe])	0.19	0.14	0.19	0.42	0.12	0.17	0.19	0.08	0.11	0.23	0.10	0.25

^a[Fe/H] values are given in the lines for [X/Fe].

^bMolecular bands used for analyses are given in the line for the number of lines used (“ N ”). CH4322: the CH λ 4322 band; CC5170: the C₂ λ 5167; CC5635: the λ 5635 band; CN4215: the CN λ 4215 band.

^bSolar elemental abundances derived by Asplund et al. (2005).

Table 11. LUMINOSITY AND ABUNDANCE RATIOS OF CARBON ISOTOPES AND NITROGEN

Object	$\log L/(L_{\odot})$	$[(C+N)/Fe]$	$^{12}C/^{13}C$	$^{12}C/N$	$^{13}C/N$
BS 16920–005	1.46	0.98–1.76	...	> 0.20	...
CS 22174–007	1.57	0.31–0.86	...	> 0.40	...
CS 22886–042	2.50	0.02–1.35	...	> 0.05	...
CS 22948–027	2.27	2.20	10 ± 3	2.00	0.20
CS 22960–053	1.87	2.50	...	0.40	...
CS 29503–010	0.13	0.97–1.12	...	> 2.51	...
CS 29528–028	0.71	2.67–3.09	...	> 0.63	...
CS 30312–100	1.47	0.44–1.22	...	> 0.20	...
CS 30322–023	2.91	1.79	...	0.05	...
CS 30338–089	2.07	1.98	12 ± 4	25.12	2.09
CS 31062–041	2.01	0.48–1.03	...	> 0.40	...
CS 29497–034	2.64	2.70	12 ± 4	5.01	0.42
HE 0206–1916	1.54	2.04	15 ± 5	12.59	0.84
HE 0400–2030	1.14	2.09	...	0.10	...
HE 0441–0652	2.74	1.32	...	12.59	...
HE 0507–1653	1.77	1.23	40^{+20}_{-10}	12.59	0.31
HE 1005–1439	2.27	2.41	...	19.95	...
HE 1157–0518	2.14	2.08	15 ± 5	15.85	1.06
HE 1319–1935	2.93	1.37	8 ± 3	39.81	4.98
HE 1429–0551	2.56	2.20	30^{+20}_{-10}	31.62	1.05
HE 1447+0102	2.51	2.39	25 ± 10	50.12	2.00
HE 1523–1155	2.50	1.83	...	6.31	...
HE 1528–0409	2.37	2.37	12 ± 5	10.00	0.83

Table 11—Continued

Object	$\log L/(L_{\odot})$	$[(C+N)/Fe]$	$^{12}C/^{13}C$	$^{12}C/N$	$^{13}C/N$
HE 2221–0453	3.55	1.75	10 ± 4	39.81	3.98
HE 2228–0706	1.61	2.23	15^{+5}_{-3}	63.10	4.21
HE 2330–0555	2.44	2.00	...	50.12	...

Table 12. ABUNDANCE RESULTS FOR NEUTRON-CAPTURE ELEMENTS in
CS 29528–028

Element	$\log \epsilon$	$[X/Fe]$	N	s.e.
Sr	1.87	1.81	2	0.20
Zr	1.98	2.25	1	0.20
La	1.20	2.93	6	0.20
Ce	1.63	2.91	1	0.20
Nd	1.54	2.95	1	0.20

Table 13. NA ABUNDANCES AND NLTE CORRECTIONS

ID	Objects	$\log \epsilon(\text{Na})_{\text{LTE}}$	Δ_{NLTE}	$\log \epsilon(\text{Na})_{\text{NLTE}}$	$[\text{Na}/\text{Fe}]_{\text{NLTE}}$
1	BS 16929–005	2.94	–0.3	2.64	–0.36
2	CS 22174–007	4.27	–0.4	3.87	–0.10
3	CS 22886–042	3.91	–0.4	3.51	–0.05
4	CS 22948–027	4.88	–0.4	4.48	0.52
5	CS 22960–053
6	CS 29503–010	5.27	...	5.27	0.16
7	CS 29528–028	5.99	–0.7	5.64	2.33
8	CS 30312–100	4.02	–0.4	3.62	–0.23
9	CS 30322–023	3.96	...	3.96	1.04
10	CS 30338–089	4.45	–0.4	4.18	0.46
11	CS 31062–041	4.23	–0.4	3.83	0.03
12	HE 0039–2635	5.03	–0.4	4.63	1.37
13	HE 0206–1916	4.82	–0.4	4.42	0.34
14	HE 0400–2030	5.15	–0.4	4.95	0.51
15	HE 0441–0652	4.42	–0.4	4.02	0.32
16	HE 0507–1653	5.22	–0.4	5.02	0.23
17	HE 1005–1439	4.19	–0.4	3.79	0.79
18	HE 1157–0518	4.57	–0.4	4.17	0.34
19	HE 1319–1935
20	HE 1429–0551	4.65	–0.3	4.35	0.65
21	HE 1447+0102	4.77	–0.4	4.37	0.67
22	HE 1523–1155
23	HE 1528–0409	4.69	–0.4	4.29	0.73
24	HE 2221–0453
25	HE 2228–0706
26	HE 2330–0555	4.37	–0.4	3.97	0.58
Na1	HD 196944	5.18	–0.4	4.78	0.86
Na2	LP 706–7	4.92	–0.7	4.22	0.6
Na3	CS 22183–015	4.03	–0.5	3.53	0.11
Na4	CS 22880–074	4.89	–0.7	4.19	–0.05
Na5	CS 22898–027	4.74	–0.5	4.24	0.33
Na6	CS 22957–027	4.56	–0.4	4.36	1.31

Table 13—Continued

ID	Objects	$\log \epsilon(\text{Na})_{\text{LTE}}$	Δ_{NLTE}	$\log \epsilon(\text{Na})_{\text{NLTE}}$	$[\text{Na}/\text{Fe}]_{\text{NLTE}}$
Na7	CS 29526–110	4.02	–0.3	3.72	–0.07
Na8	CS 30301–015	4.92	–0.3	4.62	1.09
Na9	CS 31062–050	4.2	...	4.2	0.34

Table 14. ELEMENTAL ABUNDANCES OF CEMP STARS

Object	[Fe/H]	[C/Fe]	[N/Fe]	[Na/Fe]	[Mg/Fe]	[Ca/Fe]	[Sc/Fe]	[Ti/Fe]	[Cr/Fe]	[Ni/Fe]	[Zn/Fe]	[Ba/Fe]	T_{eff}	$\log g$	$\log L/L_{\odot}$	Ref. ^a
BS 16920-005	-3.17	1.08	<2.39	-0.36	0.49	0.13	...	0.44	-0.34	-0.48	5250	2.80	1.46	
CS 22948-027	-2.21	2.12	2.43	0.52	0.55	0.57	...	0.64	-0.12	...	0.31	2.31	5000	1.90	2.27	
CS 22960-053	-3.14	2.05	3.06	...	0.65	0.43	0.49	0.54	-0.23	0.86	5200	2.10	2.14	
CS 29503-010	-1.06	1.07	<1.28	0.16	0.36	0.16	0.31	0.39	-0.12	0.01	0.32	1.50	6500	4.50	0.13	
CS 29528-028	-2.86	2.77	<3.58	2.33	1.69	0.46	0.59	0.87	...	0.26	...	3.27	6800	4.00	0.71	
CS 30322-023	-3.25	0.56	2.47	1.04	0.54	0.30	0.28	0.21	-0.36	0.59	4300	1.00	2.91	
CS 30338-089	-2.45	2.06	1.27	0.46	0.48	0.51	1.26	0.55	-0.01	...	0.46	2.22	5000	2.10	2.07	
HE 0039-2635	-2.91	2.72	2.63	1.37	1.31	0.52	...	0.46	-0.15	2.23	4900	1.50	2.64	
HE 0206-1916	-2.09	2.10	1.61	0.34	0.52	0.11	...	0.50	0.00	1.97	5200	2.70	1.54	
HE 0400-2030	-1.73	1.14	2.75	0.51	0.62	0.18	0.32	0.34	-0.08	-0.10	-0.20	1.64	5600	3.50	0.87	
HE 0441-0652	-2.47	1.38	0.89	0.32	0.35	0.31	0.14	0.31	-0.26	0.12	0.17	1.11	4900	1.40	2.74	
HE 0507-1653	-1.38	1.29	0.80	0.23	0.19	0.58	0.20	0.43	0.07	0.25	0.12	1.89	5000	2.40	1.77	
HE 1005-1439	-3.17	2.48	1.79	0.79	0.60	0.57	...	0.33	-0.38	1.06	5000	1.90	2.27	
HE 1157-0518	-2.34	2.15	1.56	0.34	0.50	0.16	...	0.09	-0.28	2.14	4900	2.00	2.14	
HE 1319-1935	-1.74	1.45	0.46	...	0.47	0.50	...	0.14	0.75	1.89	4600	1.10	2.93	
HE 1429-0551	-2.47	2.28	1.39	0.65	0.52	0.70	...	0.30	1.57	4700	1.50	2.56	
HE 1447+0102	-2.47	2.48	1.39	0.67	1.43	0.88	...	0.37	2.70	5100	1.70	2.51	
HE 1523-1155	-2.15	1.86	1.67	...	0.62	0.46	...	0.30	1.72	4800	1.60	2.50	
HE 1528-0409	-2.61	2.42	2.03	0.73	0.83	1.04	2.30	5000	1.80	2.37	
HE 2221-0453	-2.22	1.83	0.84	...	0.80	0.82	...	0.41	0.49	1.75	4400	0.40	3.55	
HE 2228-0706	-2.41	2.32	1.13	...	0.67	0.47	...	0.65	0.16	...	0.44	2.50	5100	2.60	1.61	
HE 2330-0555	-2.78	2.09	1.00	0.58	0.67	0.42	0.25	0.35	-0.10	1.22	4900	1.70	2.44	
CS 29498-043	-3.54	2.09	2.27	1.47	1.75	0.16	-0.03	0.30	-0.38	-0.36	...	-0.46	4600	1.20	2.83	1
CS 22957-027	-3.12	2.37	1.62	1.31	0.69	0.14	...	0.35	-0.21	-0.25	...	-1.23	5100	1.90	2.31	2
CS 29526-110	-2.38	2.20	1.40	-0.07	0.30	0.36	...	0.12	-0.33	-0.11	...	2.11	6500	3.20	1.43	2,3
CS 22898-027	-2.26	2.20	0.90	0.33	0.41	0.40	...	0.41	-0.10	0.02	...	2.23	6250	3.70	0.86	2,3
CS 31062-012	-2.55	2.10	1.20	0.60	0.45	0.29	...	0.36	-0.23	-0.02	...	1.98	6250	4.50	0.06	2,3
CS 22880-074	-1.93	1.30	-0.10	-0.09	0.46	0.67	...	0.41	0.20	0.13	...	1.31	5850	3.80	0.64	2,3
CS 31062-050	-2.31	2.00	1.20	0.34	0.60	0.85 ^b	...	0.42	-0.02	2.30	5600	3.00	1.37	2,3
HD 196944	-2.25	1.20	1.30	0.86	0.42	0.33	...	0.27	-0.13	0.02	0.09	1.10	5250	1.80	2.46	2,3
CS 22942-019	-2.64	2.00	0.80	...	0.58	0.68	...	0.39	0.41	1.92	5000	2.40	1.77	2,3
CS 30301-015	-2.64	1.60	1.70	1.09	0.86	0.77	...	0.23	0.33	1.45	4750	0.80	3.28	2,3
CS 30314-067	-2.85	0.50	1.20	-0.08	0.42	0.22	0.02	0.12	-0.38	-0.10	...	-0.57	4400	0.70	3.25	4
CS 29502-092	-2.76	1.00	0.70	-0.01	0.37	0.27	-0.02	0.19	...	0.16	...	-0.82	5000	2.10	2.07	4
CS 22877-001	-2.72	1.00	0.00	-0.24	0.29	0.42	-0.04	0.15	-0.29	-0.25	...	-0.49	5100	2.20	2.01	4
LP 625-44	-2.72	2.25	0.95	1.75	1.12	0.35	0.38	0.30	-0.21	-0.16	...	2.81	5500	2.50	1.84	5
CS 29497-030	-2.57	2.47	2.12	0.58	0.44	0.47	0.67	0.64	0.03	0.04	...	2.32	7000	4.10	0.66	6
CS 22881-036	-2.06	1.96	1.00	0.16	0.40	0.62	...	0.33	1.93	6200	4.00	0.55	7
CS 2148-1247	-2.32	1.91	1.65	...	0.50	0.45	0.59	0.55	-0.35	0.06	...	2.36	6380	3.90	0.69	8
CS 0024-2523	-2.72	2.60	2.10	-0.17	0.73	0.66	0.37	0.85	-0.41	1.46	6625	4.30	0.36	9
CS 22949-037	-3.99	1.17	2.57	1.44	1.58	0.35	0.10	0.35	-0.41	-0.07	0.70	-0.58	4900	1.50	2.60	10
HE 0007-1832	-2.65	2.55	1.87	...	0.76	0.32	...	0.39	...	0.02	...	0.16	6515	3.80	0.83	11
HE 0338-3945	-2.42	2.13	1.55	0.36	0.30	0.38	0.53	0.37	-0.12	0.01	...	2.41	6160	4.13	0.40	12
BS16080-175	-1.86	1.75	0.47	0.20	1.55	6240	3.70	0.86	13
BS17436-058	-1.78	1.50	1.25	0.33	0.01	1.61	5690	2.68	1.72	13
CS 22887-048	-1.70	1.84	0.48	2.00	6500	3.35	1.28	13
HE 0131-3953	-2.71	2.45	0.30	0.37	0.59	0.13	-0.21	-0.28	...	2.20	5928	3.80	0.67	14
HE 1105+0027	-2.42	2.00	0.47	0.47	0.28	0.32	0.05	-0.29	...	2.45	6132	3.50	1.03	14
HE 0202-2204	-1.98	1.16	-0.01	0.26	-0.04	-0.06	-0.40	0.04	0.03	1.41	5280	1.70	2.57	14
HE 1135+0139	-2.33	1.19	0.33	0.38	0.15	0.14	-0.24	0.01	...	1.13	5487	1.80	2.53	14

Table 14—Continued

Object	[Fe/H]	[C/Fe]	[N/Fe]	[Na/Fe]	[Mg/Fe]	[Ca/Fe]	[Sc/Fe]	[Ti/Fe]	[Cr/Fe]	[Ni/Fe]	[Zn/Fe]	[Ba/Fe]	T_{eff}	$\log g$	$\log L/L_{\odot}$	Ref. ^a
CS 22183–015	−2.75	1.92	1.77	0.11	0.54	0.96	0.56	0.56	−0.35	−0.33	...	2.04	5620	3.40	0.97	15
HE 0143–0441	−2.31	1.98	1.73	...	0.63	0.43	0.67	0.40	−0.38	−0.31	0.46	2.32	6240	3.70	0.86	15
HE 0012–1441	−2.52	1.59	0.64	...	0.91	0.42	...	0.08	−0.18	1.15	5730	3.50	0.91	15
HE 0212–0557	−2.27	1.74	1.09	...	0.04	0.14	...	0.23	−0.09	2.18	5075	2.15	2.05	15
HE 0336+0113	−2.68	2.25	1.60	...	1.04	0.42	...	0.25	−0.26	2.63	5700	3.50	0.90	15
HE 1031–0020	−2.86	1.63	2.48	...	0.50	1.12	...	0.63	−0.38	1.21	5080	2.20	2.00	15
HE 1150–0428	−3.30	2.37	2.52	...	0.34	1.03	...	0.49	−0.70	−0.61	5200	2.55	1.69	15
HE 1410+0213	−2.16	1.73	1.78	...	0.18	0.33	−0.55	0.07	5605	3.50	0.87	15
HE 1410–0004	−3.02	1.99	...	0.48	0.58	0.11	...	0.30	−0.19	1.06	4985	2.00	2.17	15
HE 1434–1442	−2.39	1.95	1.40	0.03	0.30	0.24	0.18	0.45	−0.30	0.76	...	1.23	5420	3.15	1.16	15
HE 1443+0113	−2.07	1.84	...	0.37	0.37	1.40	4945	1.85	2.30	15
HE 1509–0806	−2.91	1.98	2.23	...	0.64	0.55	...	0.62	−0.08	1.93	5185	2.50	1.73	15
HE 2158–0348	−2.70	1.87	1.52	...	0.68	0.82	...	0.54	−0.66	1.59	5215	2.50	1.74	15
HE 2232–0603	−1.85	1.22	0.47	...	0.85	0.35	0.05	0.23	−0.06	−0.65	...	1.41	5750	3.50	0.91	15

^aReferences — (1) Aoki et al. (2004); (2) Aoki et al. (2002c); (3) Aoki et al. (2002d); (4) Aoki et al. (2002b); (5) Aoki et al. (2002a); (6) Ivans et al. (2005); (7) Preston & Sneden (2001); (8) Cohen et al. (2003); (9) Lucatello et al. (2003); (10) Depagne et al. (2002); (11) Cohen et al. (2004); (12) Jonsell et al. (2006); (13) Tsangarides (2005); (14) Barklem et al. (2005); (15) Cohen et al. (2006)

^a[Ca/Fe]=0.40 is derived by the present work (see § 5.4).

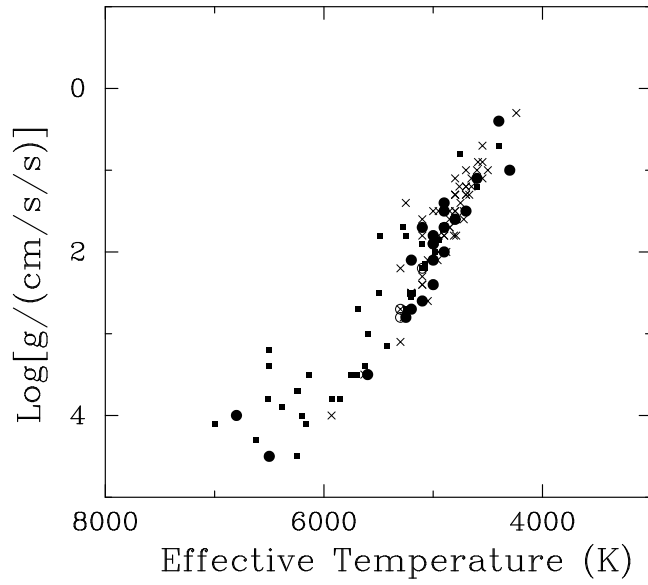


Fig. 1.— The surface gravity $\log g$ (in cgs units) determined by analyses of iron lines as a function of effective temperature. The filled circles indicate stars from our sample, while filled squares and crosses indicate other CEMP stars and non carbon-enhanced objects, respectively, studied by previous works (see text). Note the absence of horizontal-branch stars; if present, red horizontal-branch stars would be seen at $\log g \sim 2.0$.

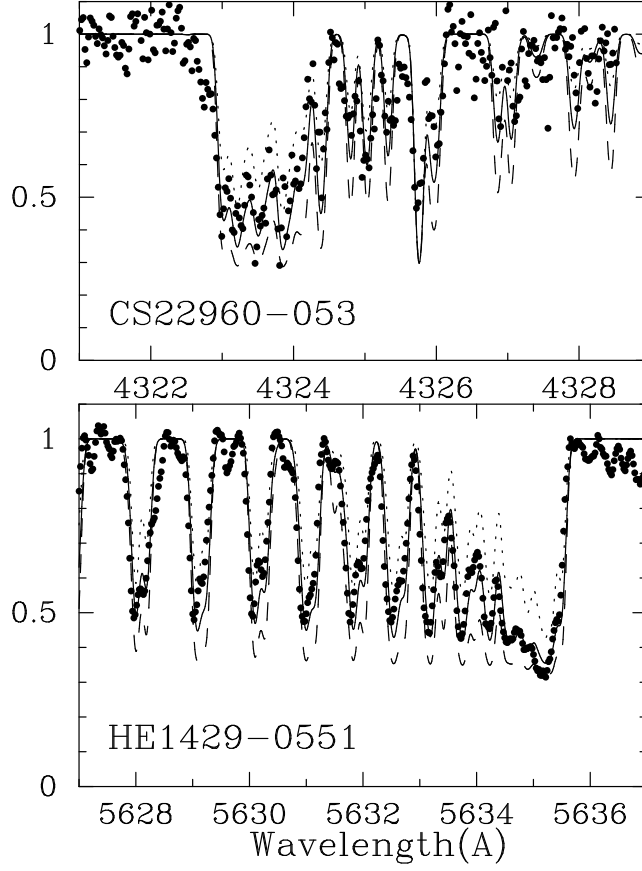


Fig. 2.— Examples of the CH and C₂ bands used for carbon abundance determinations for CS 22960-053 and HE 1429-0551, respectively. The solid lines indicate the synthetic spectra for adopted carbon abundances, while other lines show those for carbon abundances changed by ± 0.3 dex and ± 0.2 dex for CS 22960-053 and HE 1429-0551, respectively.

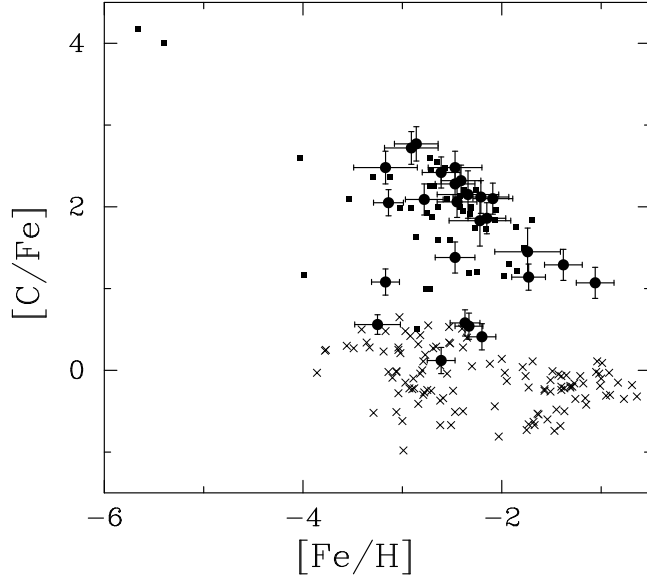


Fig. 3.— The carbon abundance ratio ($[C/Fe]$) as a function of $[Fe/H]$. The filled circles (with error bars) indicate stars from our sample, while filled squares indicate other CEMP stars. Non carbon-enhanced objects studied by previous works (Gratton et al. 2000; Cayrel et al. 2004; Honda et al. 2004b; Aoki et al. 2005) are shown by crosses.

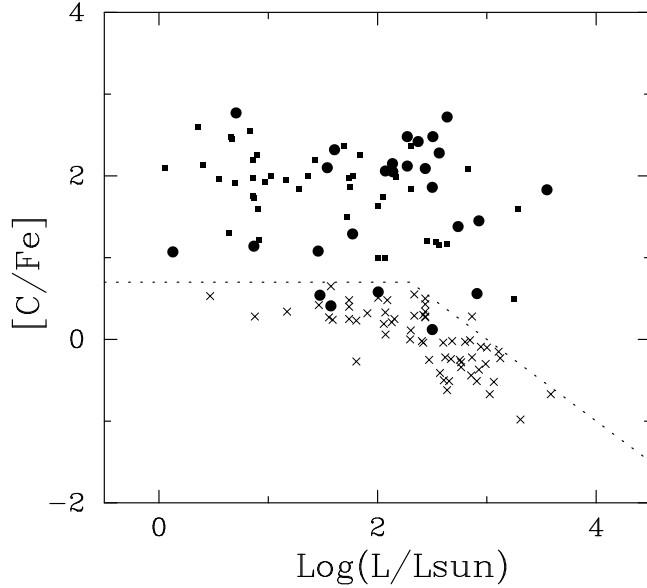


Fig. 4.— The carbon abundance ratio ($[C/Fe]$) as a function of luminosity estimated from measured effective temperatures and gravities for stars in our expanded sample. The meanings of symbols are the same as in Figure 3. The results for non carbon-enhanced stars from Cayrel et al. (2004) Honda et al. (2004b) and Aoki et al. (2005) are shown here. The dashed line indicates the dividing line between stars that we define as CEMP and the carbon-normal metal-poor stars (see text)

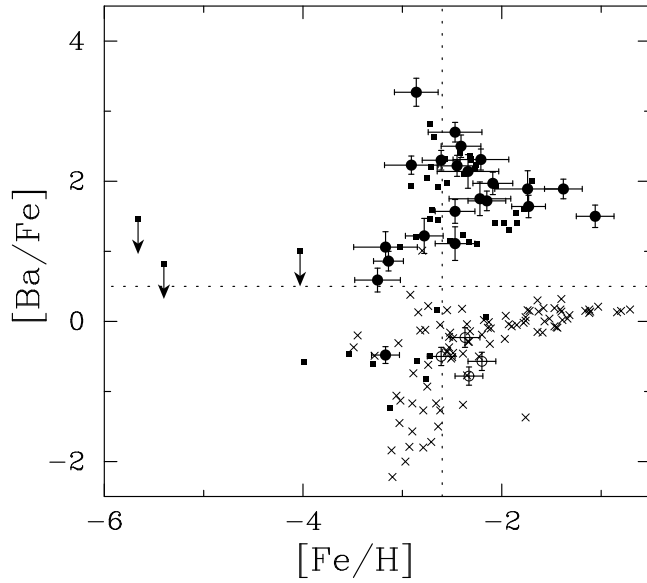


Fig. 5.— The same as Figure 3, but for $[\text{Ba}/\text{Fe}]$. The results for non carbon-enhanced stars from Stephens & Boesgaard (2002), Cayrel et al. (2004) Honda et al. (2004b) and Aoki et al. (2005) are shown here. The non carbon-enhanced objects in our sample (see text) are shown by open circles here. The upper limits of $[\text{Ba}/\text{Fe}]$ are shown for HE 1327–2326, HE 0107–5240, and G 77–61. The dotted lines indicate $[\text{Ba}/\text{Fe}] = +0.5$ and $[\text{Fe}/\text{H}] = -2.6$.

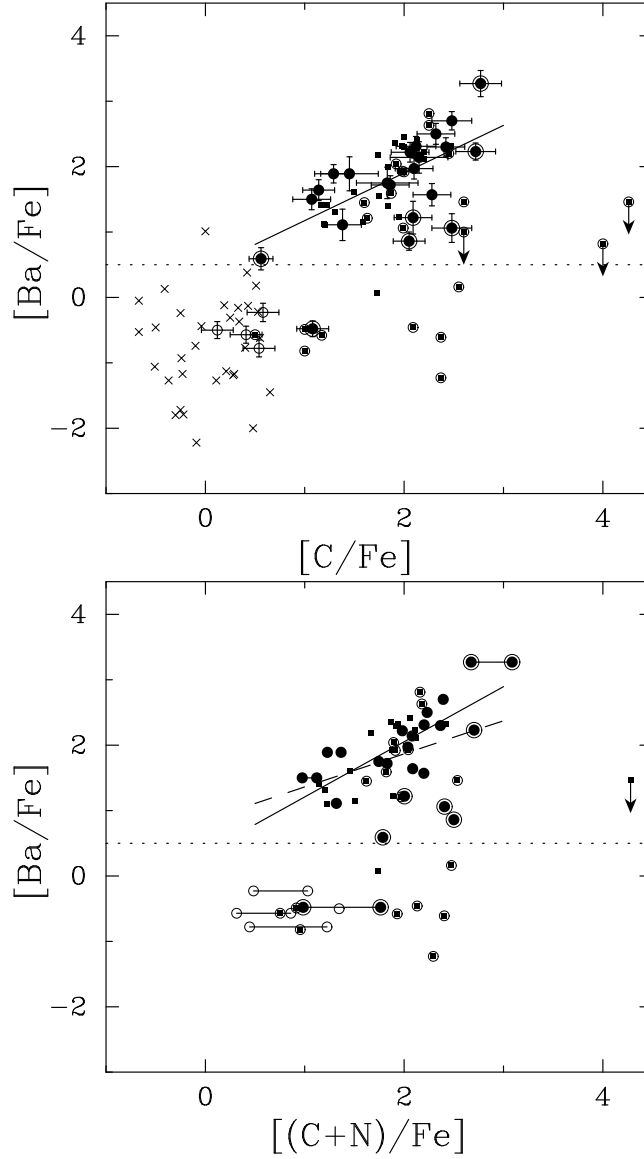


Fig. 6.— The $[\text{Ba}/\text{Fe}]$ ratio as a function of $[\text{C}/\text{Fe}]$ for stars in our expanded sample (upper panel). The meanings of the symbols are the same as in Figure 5. Stars with $[\text{Fe}/\text{H}] < -2.6$ are indicated by symbols with large open circles. The solid line indicates the least square fit for stars with $[\text{Ba}/\text{Fe}] > +0.5$ (54 stars). The lower panel is the same as the upper one, but for $[\text{Ba}/\text{Fe}]$ as a function of $[(\text{C}+\text{N})/\text{Fe}]$ instead of $[\text{C}/\text{Fe}]$. The upper and lower limits of $[(\text{C}+\text{N})/\text{Fe}]$ are connected by lines for stars for which only upper limits to the N abundance are determined (see text). The dashed line indicates the least square fit for stars with $[\text{Ba}/\text{Fe}] > +0.5$ for which N abundance is determined (44 stars), while the solid line shows that for stars having $[\text{Fe}/\text{H}] \geq -2.6$ among them (29 stars).

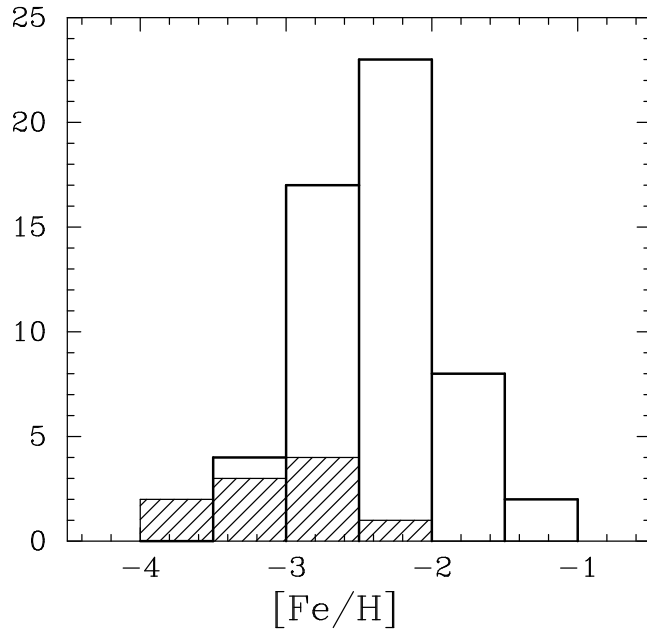


Fig. 7.— The $[\text{Fe}/\text{H}]$ distribution for CEMP stars in our expanded sample. The histogram with the “open” bars indicates the Ba-enhanced stars, while that with the hatched area is for the Ba-normal stars. There appears to be a clear difference in the distributions of $[\text{Fe}/\text{H}]$ for these two classes of stars (see text).

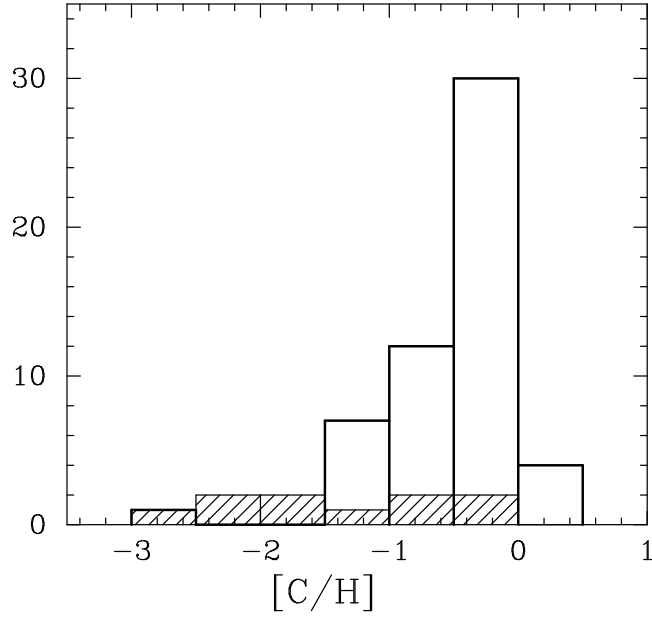


Fig. 8.— The same as Figure 7, but for the distribution of $[C/H]$ for the CEMP stars in our expanded sample. Again, there appears a clear difference in the distribution of $[C/H]$ for the Ba-enhanced and Ba-normal stars (see text).

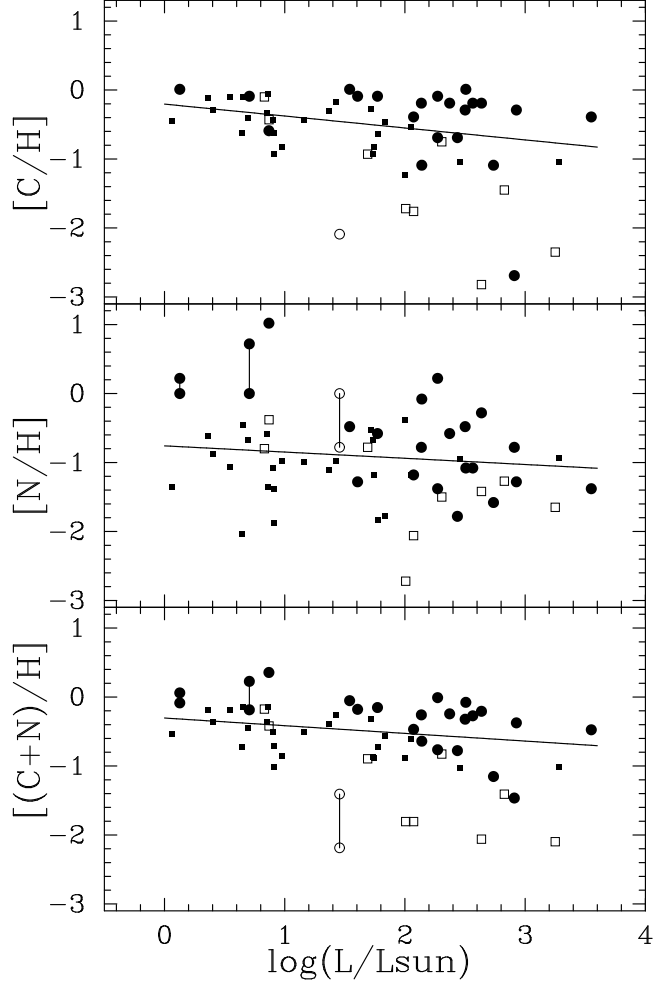


Fig. 9.— $[C/H]$ (top), $[N/H]$ (middle) and $[(C+N)/H]$ (bottom) as a function of luminosity for Ba-enhanced CEMP stars (filled symbols) and Ba-normal CEMP stars (open symbols). The solid lines indicate the least square fit to the data of Ba-enhanced CEMP stars. In the fitting to the $[N/H]$ and $[(C+N)/H]$ data, the stars for which only upper limits of N abundances are determined are ignored. Note that, on average, there exists an alteration of the surface abundances of C and C+N by about 0.6 dex, as one progresses from relatively unevolved to evolved stars at higher luminosity.

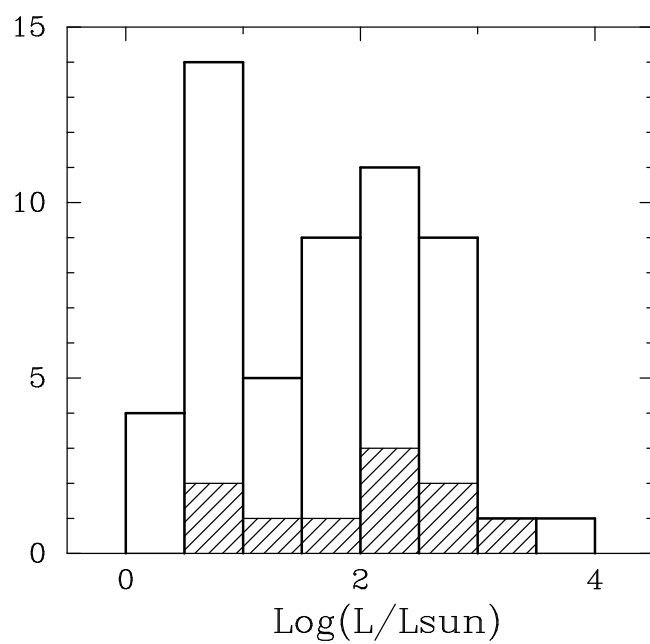


Fig. 10.— The same as Figure 7, but for the luminosity distribution for the CEMP stars in our expanded sample. The distributions of luminosity appear similar for the Ba-enhanced and Ba-normal stars (see text).

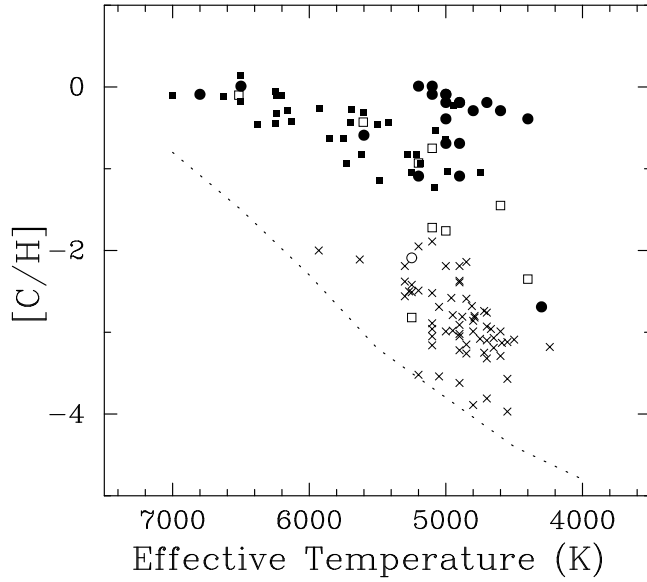


Fig. 11.— The $[C/H]$ ratio as a function of effective temperature for stars in our expanded sample. The circles and squares indicate CEMP stars identified by the present and previous work, respectively. The filled symbols are Ba-enhanced CEMP stars, while the open symbols are Ba-normal CEMP stars. The cross indicates non carbon-enhanced stars. The dotted line indicates the value of $[C/H]$ for which the depth of the CH G band reaches to about 2 % below the local continuum, as a function of temperature, estimated from synthetic spectra. Stars with $[C/H]$ below this line would not be detectable in high-resolution spectra of the quality used for this and most previous studies (see text).

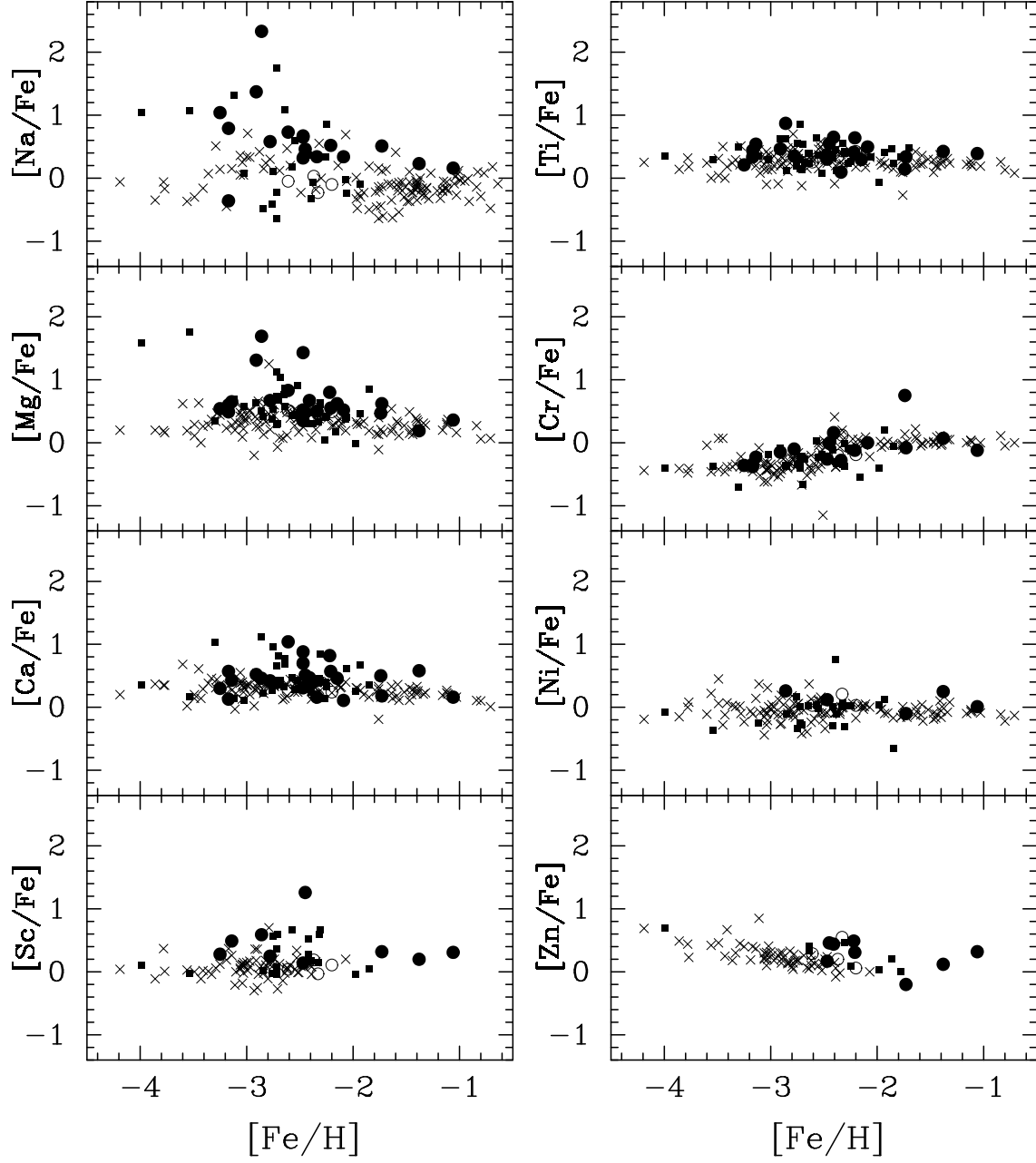


Fig. 12.— Abundance ratios of eight elements as functions of $[\text{Fe}/\text{H}]$ for stars in our expanded sample. The symbols are the same as in Figure 5.

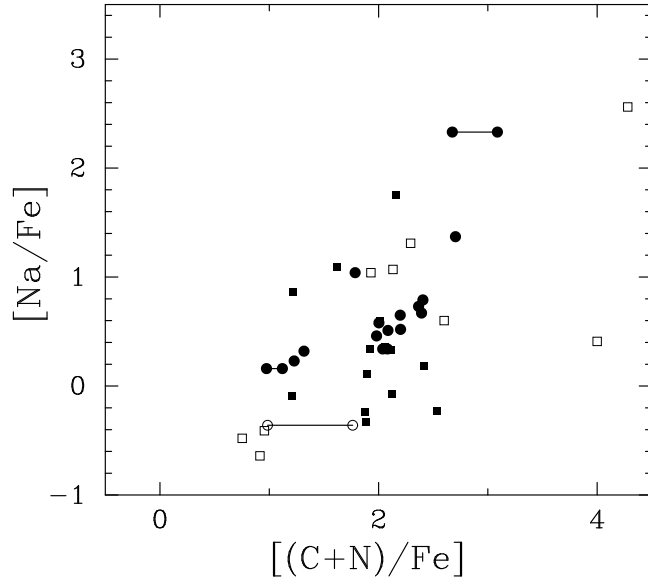


Fig. 13.— $[\text{Na}/\text{Fe}]$ ratios as a function of $[(\text{C}+\text{N})/\text{Fe}]$ for stars in our expanded sample. The filled and open circles indicate Ba-enhanced and Ba-normal CEMP stars studied by the present work, respectively, while the filled and open squares exhibit Ba-enhanced and Ba-normal CEMP stars previously studied, respectively.